ASPECTS OF MULTIPARTICLE PRODUCTION PROCESSES AT HIGH ENERGY

by

GARETH WYN PARRY

A Thesis presented for the degree of Doctor of Philosophy of the University of London, and the Diploma of Membership of Imperial college.

Department of Physics,
Imperial College of Science and Technology,
Prince Consort Road,
LONDON S.W.7.

May 1972

ABSTRACT

The study of two or more particle inclusive cross-sections is vital in order to obtain information on correlations between final state particles in a production process. We discuss the two particle inclusive cross-section for spinless equal mass particles in various regions of phase space, within the context of the Multi-Regge model. The factorization of the two particle inclusive cross-section in its extreme multi-Regge limit into the product of two single particle inclusive cross-sections, scaled by the total cross-section, is shown using a field theory model. This factorization has implications for the number distribution of produced particles. In the presence of correlations between final state particles it is argued that the Poisson distribution cannot be expected. An attempt is made to calculate the integrated correlation functions predicted by two versions of the ABFST multi-peripheral model a) the model with an input kernel given solely by low energy resonances, b) the Schizophrenic Pomeron model which includes high energy effects in the kernel. Both versions give poor results numerically. This leads to an investigation of the basic building block of the ABFST model, namely the kernel of the integral equation for the imaginary part of the forward amplitude. The usual procedure is reversed and the equation is solved for the kernel, given the imaginary part of the amplitude. The usual guess that this is related to the elastic cross-section is found to be suspect, and off-mass-shell effects are crucial.

PREFACE

The work described in this thesis was performed under the supervision of Professor P.T.Matthews and Dr. I.G.Halliday, at Imperial College, between October 1969 and May 1972. Unless otherwise stated the work is original and has not been presented for a degree of this or any other University.

The author wishes to thank his supervisors for their advice and encouragement, and in particular Dr. Halliday for his collaboration on the work described in Chapters III and VI. S.Islam also collaborated on the work of Chapter VI, and Chapter V was done with Dr. J. Dash. To these the author is indepted for their permission to incorporate this work into this thesis.

The financial assistance of the Science Research Council is gratefully acknowledged. Thanks are also due to Mrs. D.Court and Miss C.Beckstrom who assisted with the typing of the manuscript.

TABLE OF CONTENTS

	pages
Abstract	2
Preface	3
Chapter I An Introduction to Inclusive Experiments	
1.1 Motivation	6-11
1.2 Mueller's Generalized Optical Theorem	11-14
1.3 Developments	14-15
Chapter II Two Particle Inclusive Cross-Sections and the Multi-Regge Model	
2.1 Introduction	16
2.2 The Sudakov Variables and Inclusive Kinematics	17-19
2.3 The Multi-Regge Model	19-36
2.4 Discussion	36-38
Chapter III Factorization of the Two Particle Inclusive Cross-Section	
3.1 Introduction	39
3.2 The Cross-Sections	39-47
Chapter IV The Distribution of Produced Particles	
4.1 Introduction	48-50
4.2 The Multiplicity Distribution	50-53
4.3 Correlations	53-57
Chapter V Correlation Functions in the Multiperipheral Model	
5.1 The Model	58-62
5.2 The Integrated Correlation Functions	62-69
5.3 The Schizophrenic Pomeron	69-79
Footnote	80-81

pages

Chapter VI The Kernel of the ABFST Integral Equation

6.1 Introduction 82-84

6.2 The π-π Cross-Sections 84-87

6.3 Predictions of the ABFST Model 87-90

6.4 The Kernel 90-94

References 95-98

Appendix 99-100

CHAPTER I

AN INTRODUCTION TO INCLUSIVE REACTIONS

1.1 Motivation

Three of the more striking aspects of hadronic interactions at high energies are:

1) An asymptotically constant total cross-section, of which , at present accelerator energies, only a small part is elastic.

2) An average multiplicity of produced particles which increases with energy.

3) The fact that the final state particles have a restricted transverse momentum, defined with respect to the projectile beam.

From points 1) and 2) it can be seen that in order to explain hadronic reactions it is of prime importance to understand the behaviour of specific inelastic reactions. In particular it must be discovered how the various cross-sections vary with energy in such a way that the total cross-section remains constant as the energy increases. As the number of final state particles increases however, it becomes more and more difficult to display the experimental data in a meaningful way. It would therefore be useful to find some distributions in a small number of kinematic variables, which do not vanish as the energy becomes large. These distributions may each be expected to have contributions from many different specific reactions, and cannot,therefore, give us the complete answer. However, their shapes may provide us with some clues as to the sort of production processes that occur, and will certainly act as a constraint on all potential models for production amplitudes. In the terminology of Feynman(1) it may be useful to look at Inclusive Experiments- those experiments in which the momenta of a

few particles only in the final state are measured, all other combinations of particles being summed over, e.g. $p + p \to \pi^+ +$ anything or $p + p \to p + \pi^-$ + anything, as well as

Exclusive Experiments - those in which the final state is completely determined, e.g. $p + p \to \pi^+ \pi^- \pi^+ n p$. Thus the cross-section for an inclusive process includes contributions from many exclusive processes.

Interest in single particle inclusive reactions has recently been revived by the work of Feynman (1) and Benecke, et. al. (2), who argue that the single particle inclusive differential cross-sections have non-vanishing limits at high energy. However, the first investigation of single particle spectra was done by Amati, Fubini and Stanghellini (3). The invariant single particle inclusive cross-section is defined as

$$E_c \frac{d^3\sigma(s)}{d^3 p_c} = f_c(s, p_c) \qquad 1.1$$

where p_c and E_c are the three-momentum and energy of the observed particle c, when two particles a and b collide with a centre-of-mass energy squared s.

Feynman bases his arguments on the behaviour of quantum field theories at high energies, and on a picture of "hadronic brehmstrahlung" in which secondary fields are radiated from a violent collision between two particles involving exchange processes which generate exchange currents. If the collision takes place along the z-azis, the z-component of the secondary field is so compressed by Lorentz contraction that the energy it carries is distributed

evenly in p_z (the Fourier transform of a pulse is a constant), so that the spectrum of secondaries is dp_z/E independently of s. The x and y components are unaffected by the motion, so the transverse momentum distribution is also independent of s. Defining $x = 2p_z/\sqrt{s}$ we get

$$dp_z/E = dx/x \quad \text{for} \quad x^2 > O((m^2 - \underline{k}^2)/s)$$

where $p = p_z + \underline{k}$. ($\underline{k}$ spacelike)
Then $f_c(s, p_c)$ becomes $f_c(x_c, \underline{k}_c)$. In particular he argues that the function has a smooth continuation to $x_c = 0$. This point is called the pionization region, where the particles move very slowly (in the centre of mass system) compared with the incoming particles. This argument is expected to hold for small x_c, but by considering the behaviour of the field theoretic amplitude for producing a particle of momentum p_c in the final state, he extends the result to all values of x_c. This is Feynman scaling, i.e.

$$f_c(s, p_c) \xrightarrow[s \to \infty]{} f_c(x_c, \underline{k}_c)$$

the inclusive cross-section reaches a non-zero limit dependent only on x_c and $\underline{k}_c$ at high energies.

Benecke, et. al. (2) assume that in a hadronic collision the hadrons shatter into fragments as they pass through each other. The hadrons in their picture are semi-transparent objects. In the laboratory frame the fragments of the projectile are expected to have a certain fraction of the momentum of the projectile, and as this increases without limit as s increases the momentum distribution of these particles will not have a limiting distribution. However,

in the laboratory frame, the target sees the projectile as a Lorentz contracted disc. Once the apparent thickness of the disc has reached a certain minimum, $\sim O(1/\sqrt{s})$, further decrease, obtained by increasing s, will not be expected to affect the fragmentation of the target at least for a bounded $|p_c|$. The inclusive cross-section for fragments of the target for a certain restricted range of $|p_c|$ is consequently expected to attain a constant value as s increases. This argument is supposed to be valid for those p_c such that $|p_c|/\sqrt{s} \to 0$ where p_c is measured in the target rest frame. These fragments cannot be confused with fragments of the projectile. The same statements can be made about the fragments of the projectile in the projectile rest frame. This is the hypothesis of limiting fragmentation. No predictions are made for those fragments which have $|p_c|/\sqrt{s} \to 0$ when p_c is measured in the centre of mass frame. Benecke, et. al. argue that they prefer that no particles be produced in this region such that they are not fragments of either target or projectile, i.e. no pionized particles. However, this is not excluded by their picture.

Feynman discusses his hypothesis in the centre-of-mass frame and Benecke, et. al. discuss theirs in the laboratory frame. A useful variable which connects the two pictures, again due to Feynman, is the rapidity y.

$$y = \sinh^{-1}\left[\frac{p_z}{(m^2 - \underline{k}^2)^{1/2}}\right]$$

in any given frame. In any other frame connected by a Lorentz transformation in the z direction, the rapidity is given by $y + Y$ where Y is the rapidity associated with the Lorentz transformation between the two frames. On transformation to rapidity, the target fragmentation region $x < 0$ is mapped into

a finite length of rapidity of constant length as s increases, as is the projectile fragmentation region. The distance between the two regions grows logarithmically with s as s increases (4). The Feynman and Benecke pictures then look like Figs. 1a, 1b respectively at fixed K.

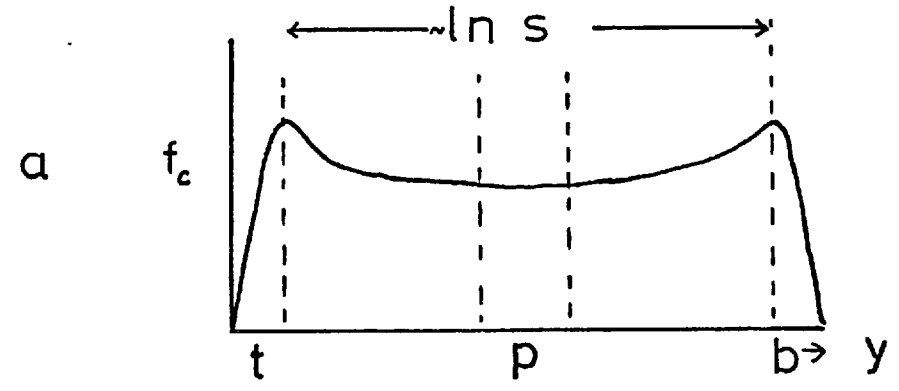

Fig. 1

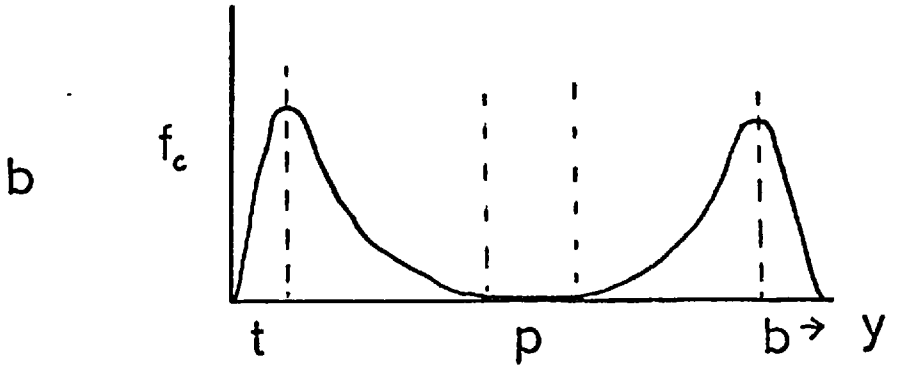

The regions marked t, p, and b are the target fragmentation, pionization, and beam fragmentation regions respectively. In both pictures the curves in sections t and b are s independent and here both conjectures agree. However in the Feynman picture the central region has a constant height as s increases, over a region, p, small compared with $\log S^{\frac{1}{2}}$. No prediction is made by Benecke et al in this region. Absence of this plateau will rule out Feynman's picture, but its presence does not rule out that of Benecke.

Feynman scaling has been shown to be a property of multiperipheral models (3, 5, 6). These calculations involve

adding up all the exclusive cross-sections that contribute to the inclusive cross-section. A short cut to this approach has been proposed by Mueller (7) whose generalized optical theorem we discuss in the next section.

1.2 Mueller's Generalized Optical Theorem

Elastic unitarity gives

$$\text{Disc.}_s \left(T_{2\to 2}(s,t=0) \right) = \sum_n T_{2\to n} T^{+}_{2\to n} \qquad 1.2$$

where Disc._s is the discontinuity in the s variable, T is the T-matrix, and $\sum_n$ means the sum over n of the integral over n-particle phase space. Pictorially we write this equation as

Disc._s [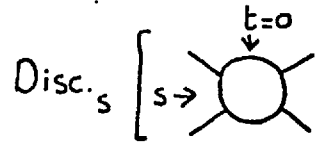] $= \sum_n$ 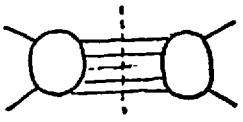 1.3

The right hand side of Eqtn. 1.3 can now be recognized as $F.\ \sigma_{tot}(s)$ where F is the flux factor. This gives us the optical theorem, namely

$$\text{Disc.}_s \left[T_{2\to 2}(s,t=0) \right] = F.\ \sigma_{tot.}(s) \qquad 1.4$$

In an inclusive reaction we are considering the process $a+b\to c+$ anything (Fig. 2). If the crossing properties of the

Fig. 2

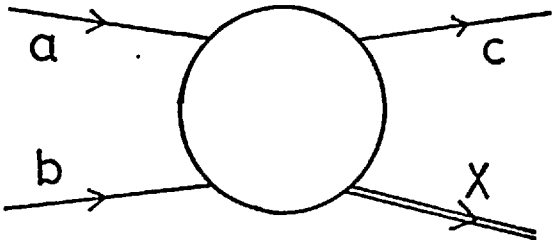

amplitude are suffiently smooth, this may be transformed to $a+b+\bar{c}\to$ anything. Thecross-section for this process is then

$$E_c \frac{d^3\sigma}{d^3p_c} = \frac{1}{F} \sum_n \left[\right] \qquad 1.5$$

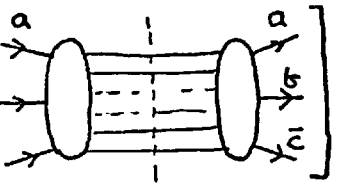

By analogy with elastic unitarity we might expect this to be $1/F$ times the discontinuity in the missing mass squared X^2 of the $3\to3$ amplitude (Fig. 3).(The + and - refer to whether the relevant sub-energy is taken above or below its cut.) The amplitude is an unphysical amplitude since the sub-energy $S_{b\bar{c}}$ is negative. The proof

Fig. 3

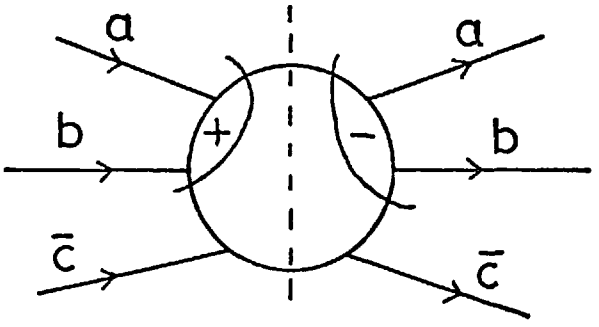

that the inclusive cross-section can indeed be identified with the discontinuity of this $3\to3$ amplitude has been discussed by Stapp (8), Tan (9), and Polkinghorne (10) within the context of the analytic S-matrix theory (11).

As $s \to \infty$ therefore we have, since $F \sim s$,

$$E_c \frac{d^3\sigma}{d^3p_c} \sim \frac{1}{s} \text{ Disc.}_{X^2} \left[\right] \qquad 1.6$$

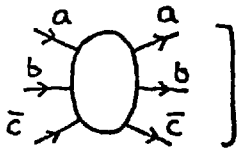

Since the $3\to3$ amplitude is not a physical amplitude, this technique is a theoretical tool only, unlike the standard optical theorem which relates two physical objects.

Mueller next examines two kinematic limits of this process.

He expands the 3→3 amplitude using O(2,1) expansions in the variables which go infinite. The leading asymptotic behaviour is then assumed to be given by the leading J-plane poles. These poles are assumed to be same as those which occur in two-body reactions, and in this case, since the quantum numbers exchanged are zero, it is the Pomeron which is the leading pole. Its intercept is taken to be one.

a) $s_{ab} = (p_a + p_b)^2 \to \infty$, $s_{ac} = (p_a - p_c)^2 \to -\infty$,

$s_{bc} = (p_b - p_c)^2 \to -\infty$,

Here a double O(2,1) expansion is appropriate. If p_c is written as $p_z + K$ as before, then Mueller obtains

$$f_c(p_c, s) \underset{s\to\infty}{\to} f(K^2) \qquad 1.7$$

which is Feynman;s pionization result if $f(K^2) \neq 0$. Diagramatically this corresponds to the double Regge pole limit of the 3→3 amplitude as in Fig. 4a .

Fig. 4

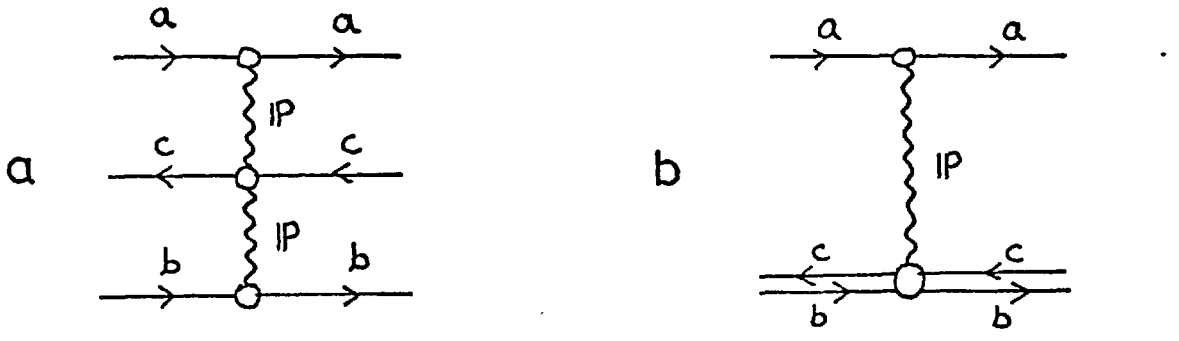

b) $s_{ab} \to \infty$, $s_{ac} \to -\infty$,

s_{bc} finite ,

Here a single O(2,1) expansion in the variable s_{ac} is used, resulting in

$$f_c(p_c, s) \underset{s\to\infty}{\to} \gamma(K, p_z) \qquad 1.8$$

where p_c is measured in the rest frame of b and is finite. This is the hypothesis of limiting fragmentation. Diagramatically this

corresponds to Fig. 4b.

Mueller also calculates the mean multipicity of produced particles to be of the form $a\log s + b$, which is the result expected if the cross-section scales in the Feynman sense. We will return to this point in Chapter IV.

I.3 Developments

The work of Mueller has precipitated a great volume of work on single particle inclusive distributions, both theoretical and experimental. As examples of the theoretical work we quote de-Tar et al (12), who catalogue the different asymptotic limits, and Chan Hong Mo et al (13) who, guided by duality and the fact that in elastic two body reactions, those with exotic s-channels are Pomeron dominated at lower energies than those with non-exotic s-channels, propose a method of chosing suitable reactions which might scale at relatively low energies. They argue that in the fragmentation region of b, $b\bar{c}$ may be regarded as a single particle, and if $ab\bar{c}$ is exotic the Pomeron will dominate at low energies, since there will be no secondary Regge poles coupling to the system, by analogy with Harari-Freund duality (14,15). Consequently scaling should occur at much lower energies than in the non-exotic case where Regge poles can couple. Reviews of the theoretical developments have been given by Arnold (16) and Berger (17, 18) among others.

The experimental situation is at the moment changeable, so we will not draw any conclusions, but merely list some of the more interesting published results. Scaling has been shown to work at low energies (8 -16 GeV/c)in $\pi^+ p \to \pi^- +$ anything, but not for $\pi^+ p \to \pi^+ +$ anything (19) in the region away from x=0, in agreement with the conjecture of Chan et al. The factorization of the cross-section proposed by Mueller i.e.

$$\frac{\sigma_{ab\to c}}{\sigma_{tot\,ab}} = \frac{\sigma_{ad\to c}}{\sigma_{tot.\,ad}}$$ in the fragmentation region of a seems to be roughly valid (20). Scaling in the fragmentation region appears to work (21). The experiment of Barbiellini et al (22) shows that the plateau in the central region exists, but that it is still energy dependent at I.S.R. energies. For a more detailed account of the experimental situation we refer to Berger (17,18).

While single particle spectra can give much information on what sort of processes occur e.g. whether pionization exists, if we are to find out how one final state particle is affected by another in a more specific way, we must look at experiments where more than one particle is observed. This leads us to consider the two particle inclusive reactions. This is the subject of the next three chapters. In Chapter II we investigate the behaviour of the two particle inclusive cross-sections in different kinematic regions, using the Multi-Regge model as a guide. In Chapter III we prove, using a field theory model, the factorization of the two particle inclusive cross-section in its extreme multi-Regge limit, and in Chapter IV we discuss some implications this has on the multiplicity distribution of produced particles.

CHAPTER II

TWO PARTICLE INCLUSIVE CROSS-SECTIONS AND THE MULTI-REGGE MODEL

2.1 Introduction

In this chapter we investigate the two particle inclusive cross-sections in various kinematic regions (23). We write down the multi-Regge amplitude appropriate to each limit. This enables us to extract the dependence on the infinite sub-energies s_i in the form $s_i^{\alpha(t_i)}$ where $\alpha(t_i)$ is a Regge pole trajectory. The residue function is then an unknown function of the remaining finite variables. We assume for simplicity that all the particles have equal mass and are spinless.

We are considering the process $a+b \to c+d+X$ (Fig. 1)

Fig. 1

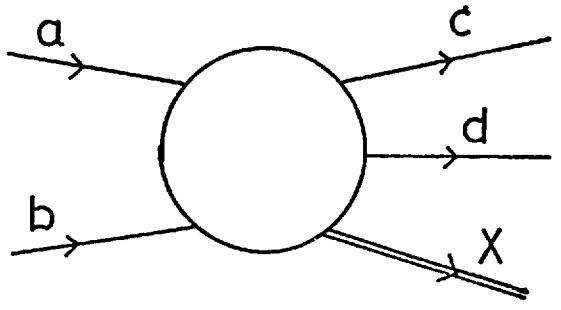

For an n-body process there 3n-10 independent invariants that can be formed from the momenta of the particles. We can regard Fig. 1 as a five point amplitude, but with one of the masses, X^2, variable. Our scattering amplitude and hence our inclusive cross-section is therefore dependent on six independent variables. Discussion of the kinematics of production processes has been shown to be very much simplified by the use of a set of variables first introduced by Sudakov (24,25). We discuss the Sudakov variables briefly in the next section.

2.2 The Sudakov Variables and Inclusive Kinematics

The variables are defined in the following manner (25). Suppose we are dealing with a $2\to n$ process (Fig. 2), the outcoming particles are ordered such that the q_{i_z}, the component of q_i parallel to $p_a - p_b$ in the Centre of Mass frame, decrease (from positive to negative values) from q_{1_z} to q_{n_z} i.e. $q_{1_z} > q_{2_z} > \cdots > q_{n_z}$.

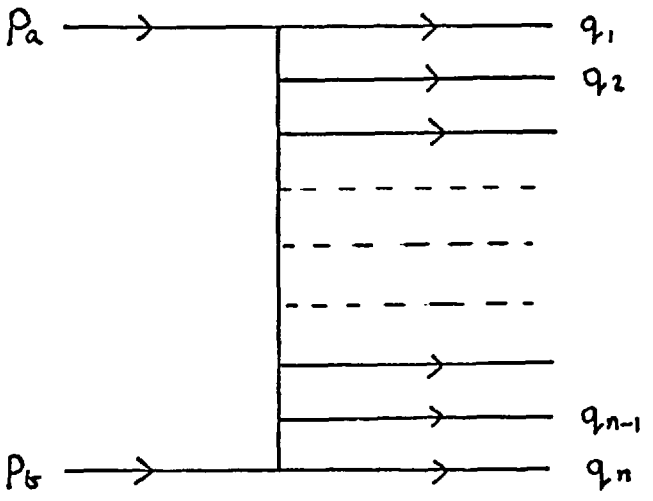

Fig. 2

The component of the momentum q_i perpendicular to $p_a - p_b$ is denoted by K_i . We have

$$K_i \cdot p_a = K_i \cdot p_b = 0 \qquad \text{with } K_i^2 < 0 \text{ (spacelike)} \qquad 2.1$$

Define

$$p_1 = p_a - m^2 p_b / s$$
$$p_2 = p_b - m^2 p_a / s \qquad 2.2$$

where m is the mass of the particles. Then

$$p_1^2 = p_2^2 \sim 2/s$$

and $$2\, p_1 \cdot p_2 \sim s \qquad \text{as} \quad s \to \infty \,. \qquad 2.3$$

The Sudakov variables (α_i , β_i , K_i) are defined by the relation

$$q_i = \alpha_i p_1 + \beta_i p_2 + K_i \qquad 2.4$$

Energy momentum conservation becomes

$$\sum_{i=1}^{n} \alpha_i = 1 + O(1/s)$$
$$\sum_{i=1}^{n} \beta_i = 1 + O(1/s) \qquad 2.5$$

and the mass shell constraint $q_i^2 = m^2$ becomes

$$\alpha_i \beta_i s + \underline{K}_i^2 = m^2 + O(1/s) \qquad 2.6$$

From now on we will take $m^2=1$.

Equation 2.6 implies that $\alpha_i \beta_i > 0$. q_{i_0} in the Centre of Mass frame of a and b is $\sim(\alpha_i + \beta_i)\sqrt{s}/2$. These two relations ensure that α_i and β_i are positive. It is clear from (2.5) that since α_i and β_i are both positive for all i, the maximum value of either is 1. We have

$$O(\tfrac{1}{s}) \leqslant \alpha_i \leqslant 1 \quad , \quad O(\tfrac{1}{s}) \leqslant \beta_i \leqslant 1 \quad . \qquad 2.7$$

Then, for example, we obtain

$$s_i = (q_i + q_{i+1})^2 = s(\alpha_i + \alpha_{i+1})(\beta_i + \beta_{i+1}) + (\underline{K}_i + \underline{K}_{i+1})^2$$

and $$t_i = (p_a - \sum_{j=1}^{i} q_j)^2 = -s(1 - \sum_{j=1}^{i} \alpha_j)(\sum_{j=1}^{i} \beta_j) + \qquad 2.8$$

$$+ (\sum_{j=1}^{i} \underline{K}_j)^2 .$$

We wish to consider the process $a+b \to c+d+X$. Let us assume that c and d are ordered in the above sense and are represented by $(\alpha_1, \beta_1, \underline{K}_1)$ and $(\alpha_2, \beta_2, \underline{K}_2)$. The energy momentum constraint becomes

$$O(\tfrac{1}{s}) \leqslant \alpha_1 + \alpha_2 \leqslant 1$$

$$O(\tfrac{1}{s}) \leqslant \beta_1 + \beta_2 \leqslant 1 \qquad 2.9$$

where the equalities hold when X is nothing. In general some of the momentum will be carried away by X.

We define the kinematic variables in the following way

$$s = (a+b)^2$$

$$s_{cd} = (c+d)^2$$

$$s_{ac} = (a-c)^2$$

$$s_{bac} = (a+b-c)^2 = s_{dx}$$

$$s_{bx} = (b-x)^2 = (a-c-d)^2$$

2.10

where a is the momentum of particle a etc. Thus $S_{ij} = (i \pm j)^2$ where the positive sign is used when both particles are incoming or outgoing, and the negative sign when one is incoming, the other outgoing.

These become, in terms of Sudakov variables

$$S_{cd} = (\alpha_1+\alpha_2)(\beta_1+\beta_2)s + (\underline{K}_1+\underline{K}_2)^2,$$

$$S_{ac} = -(1-\alpha_1)\beta_1 s + \underline{K}_1^2 \qquad 2.11$$

etc.

These expressions are valid as $s\to\infty$, i.e. when terms proportional to $1/s$ may be neglected with respect to constants.

Throughout this chapter we will assume that $\underline{K}_1^2$, $\underline{K}_2^2$ and $\underline{K}_1.\underline{K}_2$ are bounded and finite as indicated by experiment.

2.3 The Multi-Regge Model

The multi-Regge model for production amplitudes (26) is supposed to be valid in the phase space region where all the sub-energies of the ordered outgoing particles are large, and all the momentum transfers are small. In terms of Fig. 3 all $s_i\to\infty$, and all t_i are small. The production amplitude is then written as

$$G(t_1).\, s_1^{\alpha(t_1)}.\, g\left(t_1, t_2, \frac{s_1 s_2}{s_{12}}\right).\, s_2^{\alpha(t_2)} \times$$

$$.\, g\left(t_2, t_3, \frac{s_2 s_3}{s_{23}}\right) ..... s_{n-1}^{\alpha(t_{n-1})}.\, G(t_{n-1}) \qquad 2.12$$

G(t) is the coupling of two particles to a Reggeon and g is the coupling of two Reggeons to a particle which depends on the "masses" t_1, t_2 of the Reggeons and the angle between the planes defined by the momenta of one of the Reggeons and the particle. This is equivalent to a dependence on $s_1 s_2/s_{12}$, t_1 and t_2 or alternatively $\underline{K}_1^2$, $\underline{K}_2^2$ and $\underline{K}_1.\underline{K}_2$. The kinematics of the multi-Regge region in terms of Sudakov variables has been discussed by Halliday and Saunders (25) and will be used frequently

Fig. 3

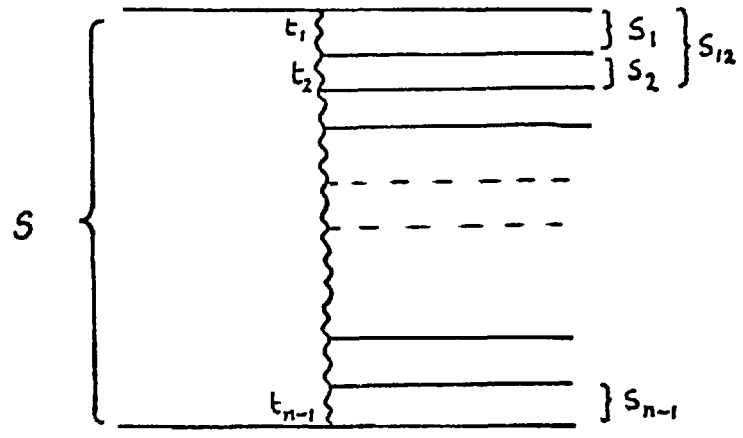

in this chapter.

The regions of phase space we will discuss fall into three main categories depending on whether X^2 is of the same order as s, much smaller than s but still large, or very small. We will discuss these cases separately.

1) X^2 fixed small as $s \to \infty$

For certain kinematic configurations we may regard all the momentum in "X" as emerging from one region of the diagram corresponding to the production amplitude. Then we may regard "X" as a single particle of mass X^2. We are then concerned with a $2 \to 3$ process and the two particle inclusive cross-section is given by

$$E_c E_d \frac{d^6\sigma}{d^3q_c\, d^3q_d} \sim \frac{1}{s} \left| A_{a+b \to c+d+X} \right|^2 \qquad 2.13$$

$1/s$ is the flux factor, E_c and E_d are the energies of particles c and d with 3-momenta q_c and q_d respectively, and $A_{a+b \to c+d+X}$ is the production amplitude. We may draw four multi-Regge diagrams to represent these limits (Figs. 4a→4d).

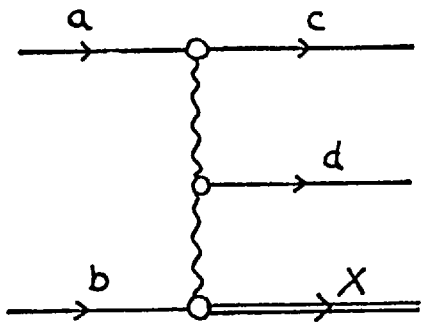

a

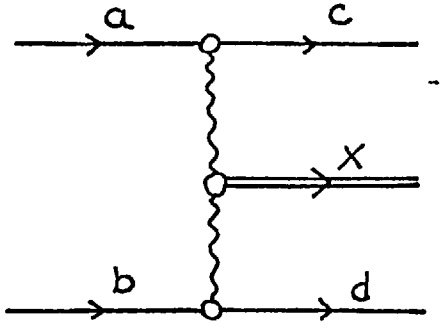

b

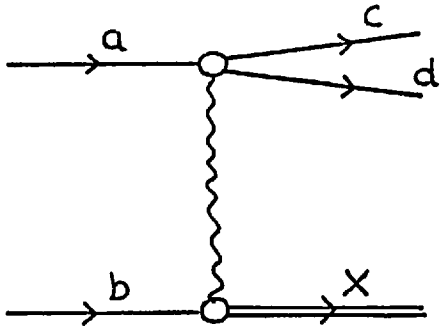

c

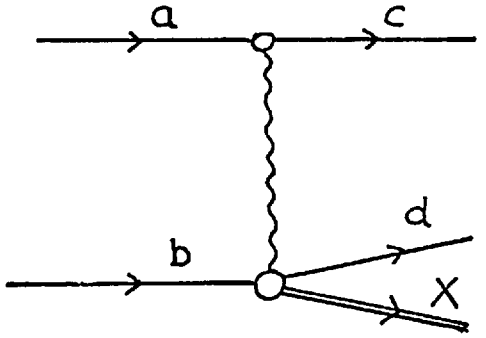

d

Fig. 4

For convenience we denote $E_c E_d \frac{d^6\sigma}{d^3q_c\, d^3q_d}$ by F

throughout this chapter.

a) The amplitude represented by Fig. 4a is valid when

s_{ac} fixed small, s_{acd} fixed small,

$s_{cd} \to \infty$ $\quad s_{dx} = s_{acb} \to \infty$

However in the multi-Regge configuration s_{cd} and s_{dx} cannot go infinite in an arbitrary fashion, as shown below. In the multi-Regge limit for a 2→n process the α_i and β_i are constrained in a very specific manner (25), namely

$\alpha_1 >> \alpha_2 >> \alpha_3 >> \ldots\ldots >> \alpha_n$ such that $\alpha_i/\alpha_{i+1} \to \infty$

and $\beta_1 << \beta_2 << \beta_3 << \ldots\ldots << \beta_n$ such that $\beta_{i+1}/\beta_i \to \infty$

with $\alpha_1 \to 1$, $\beta_1 \sim O(1/s)$

$\beta_n \to 1$, $\alpha_n \sim O(1/s)$ 2.14

Then in our case $s_{cd} \sim \alpha_1 \beta_2 s \sim \beta_2 s$

$s_{dx} \sim \alpha_2 \cdot (1-\beta_1-\beta_2) s \sim \alpha_2 s$ 2.15

and $s_{cd}\, s_{dx}/s = \alpha_2 \beta_2 s = (1-\underline{k}_2^2)$

using the mass constraint.

Thus in this multi-Regge limit we also need the constraint

$s_{cd} \cdot s_{dx}/s$ is fixed and finite as $s \to \infty$

The multi-Regge amplitude for this case is

$$A = s_{cd}^{\alpha(s_{ac})}\, s_{dx}^{\alpha(s_{acd})}\, f\left(s_{ac}, s_{acd}, X^2, \frac{s_{cd}\, s_{dx}}{s}\right) \quad 2.16$$

$\alpha(s_{ac})$ is the Regge pole trajectory coupling to the $a\bar{c}$ system, and $\alpha(s_{acd})$ that coupling to the quantum numbers of the $a\bar{c}\bar{d}$ system. f is the residue function which if we write down the factorized form suggested by the multi-Regge model (27) is

$$f_1(s_{ac})\, f_2\left(s_{ac}, s_{acd}, \frac{s_{cd}\, s_{dx}}{s}\right)\, f_3(s_{acd}, X^2) \quad 2.17$$

$$F \sim \frac{1}{S} S_{cd}^{2\alpha(S_{ac})} S_{dx}^{2\alpha(S_{acd})} \cdot f^2\left(S_{ac}, S_{acd}, X^2, \frac{S_{cd}S_{dx}}{S}\right)$$

$$= S^{2\alpha(S_{acd})-1} S_{cd}^{2\alpha(S_{ac})-2\alpha(S_{acd})} \cdot g\left(S_{ac}, S_{acd}, X^2, \frac{S_{cd}S_{dx}}{S}\right) \qquad 2.18$$

where $\left(\frac{S_{cd}S_{dx}}{S}\right)^{2\alpha(S_{acd})}$ is absorbed into f^2 to give g.

Assuming factorization we may write this as

$$S^{2\alpha(S_{acd}-1)} \cdot S_{cd}^{2\alpha(S_{ac})-2\alpha(S_{acd})} \cdot \beta_1(S_{ac}) \times$$

$$\beta_2\left(S_{ac}, S_{acd}, \frac{S_{cd}S_{dx}}{S}\right) \cdot \beta_2(S_{acd}, X^2) \qquad 2.19$$

b) The region of validity of Fig. 4b is

$S_{cx} \to \infty$ $\qquad$ $S_{dx} \to \infty$

S_{ac} fixed small, $\qquad$ S_{bd} fixed small,

such that $\frac{S_{cx}S_{dx}}{S}$ is fixed small.

As above we can write

$$F \sim S^{2\alpha(S_{bd})-1} \cdot S_{cx}^{2\alpha(S_{ac})-2\alpha(S_{bd})} \cdot \beta_1(S_{ac}) \times$$

$$\beta_2\left(S_{ac}, S_{bd}, \frac{S_{cx}S_{dx}}{S}, X^2\right) \cdot \beta_3(S_{bd}) \qquad 2.20$$

c) Fig. 4c is the single Regge limit

$S_{dx} \to \infty$, $\qquad$ $S_{bd} \to -\infty$

S_{acd} fixed small, $\qquad$ S_{cd} fixed small,

such that S_{dx}/S is fixed small.

Here $\alpha_1 \gtrsim \alpha_2$ and $\beta_1 \lesssim \beta_2$ with $1-\alpha_1-\alpha_2 \sim O\left(\frac{1}{S}\right)$

and $1-\beta_1-\beta_2 \to 1$ $\qquad$ 2.21

$$S_{dx} = \alpha_2(1-\beta_1-\beta_2)S + \underline{K}_1^2 \qquad 2.22$$

The condition that S_{dx}/S be constant implies that $\alpha_2(1-\beta_1-\beta_2)$ be constant, which in turn implies that both α_2 and $1-\beta_1-\beta_2$ be constant. So this condition, combined with the

other conditions ensures that we are in the region of phase space described by Fig. 4c. In particular all the momentum in X may be regarded as emerging from one point in the diagram since

$\alpha_1 + \alpha_2 \gg 1 - \alpha_1 - \alpha_2$ ($\alpha_1 \sim \alpha_2 \sim$ constant, $1-\alpha_1-\alpha_2 \sim o(\frac{1}{s})$)

This condition on X means that its position on the diagram is unambiguous, and we do not confuse our region with that where Fig.5 is appropriate.

Fig. 5

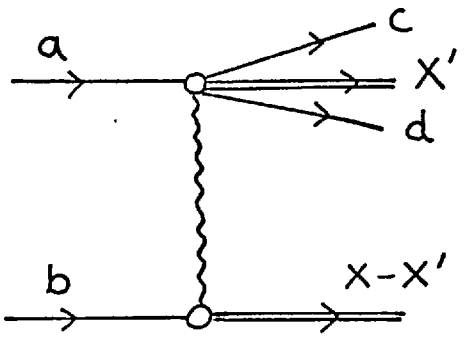

$$F \sim s^{2\alpha(s_{acd})-1} \cdot \beta_1(s_{acd}, s_{cd}, s_{ac}) \cdot \beta_2(X^2, s_{acd}) \quad 2.23$$

d) Fig. 4d is valid when

$s_{cd} \to \infty$, s_{dx} fixed small,

s_{ac} fixed small, s_{acd} fixed small,

such that s_{cd}/s is fixed small.

$$F \sim s^{2\alpha(s_{ac})-1} \cdot \beta_1(s_{ac}) \cdot f\left(s_{ac}, X^2, s_{dx}, s_{acd}, \frac{s_{cd}}{s}\right) \quad 2.24$$

This may be compared with a suitable two-body high energy process, and by factorization will give information on the fragmentation of particle b into d together with other matter of low invariant mass squared,

2) Now let us consider those kinematic limits where $X^2 \to \infty$,but in such a way that s/X^2 remains finite. Here it proves useful to use the Generalized Optical Theorem of Mueller,relating the inclusive cross-section to the discontinuity of the elastic 4→4 amplitude in

the X^2 variable. We make the same approximations as Mueller, in that we assume that the Regge poles dominating the 4→4 amplitude are the same as those in two body processes. In particular we assume factorization of the Pomeron. The multi-Regge model is then used to extract the dependence on the infinite energy variables.

We draw five different diagrams to describe this limit (Fig. 6a →6e)

a) This diagram represents the limit

$$s_{ac} \to -\infty \quad , \quad s_{bd} \to -\infty \, ,$$
$$s_{cd} \to \infty$$

Again, since our particles are ordered these sub-energies cannot all go infinite arbitrarily. Asusual, assuming $\underline{K}_1^2$, $\underline{K}_2^2$, and $\underline{K}_1 . \underline{K}_2$ are finite we have

$$\begin{aligned} s_{ac} &= -\beta_1 s \\ s_{cd} &= (\alpha_1 \beta_2 + \alpha_2 \beta_1) s \\ s_{db} &= -\alpha_2 s \end{aligned} \qquad 2.26$$

giving
$$s_{ac} . s_{cd} . s_{db} = \alpha_2 \beta_1 (\alpha_1 \beta_2 + \alpha_2 \beta_1) s^3$$
$$\sim (1 - \underline{K}_1^2)(1 - \underline{K}_2^2) s \left(1 + \frac{\alpha_2 \beta_1}{\alpha_1 \beta_2}\right) \qquad 2.27$$

to leading order in s.

To ensure that s_{cd}, s_{ac}, and s_{db} are all infinite we have

$$\beta_1 \sim \frac{1}{s^{1-n}} \quad , \quad \alpha_2 \sim \frac{1}{s^m} \qquad 0 < n, m < 1$$

with $\alpha_1 \gg \alpha_2$ (if $\alpha_1 \sim \alpha_2$ then $\beta_1 \sim \beta_2$ and $(\alpha_1 \beta_2 + \alpha_2 \beta_1) \sim O(1/s)$) therefore $n < m$

giving
$$s_{ac} . s_{cd} . s_{db} \sim (1 - \underline{K}_1^2)(1 - \underline{K}_2^2) s \left(1 + s^{2(n-m)}\right)$$
$$\sim (1 - \underline{K}_1^2)(1 - \underline{K}_2^2) s \qquad 2.28$$

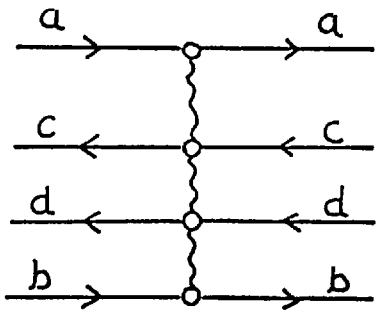

a

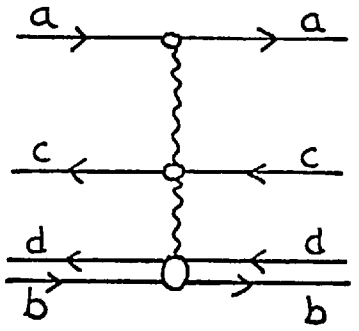

b

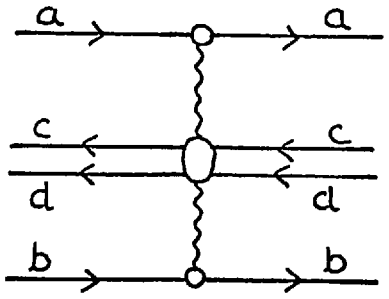

c

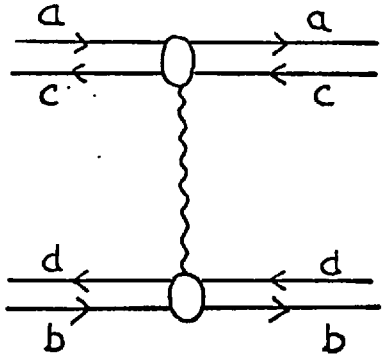

d

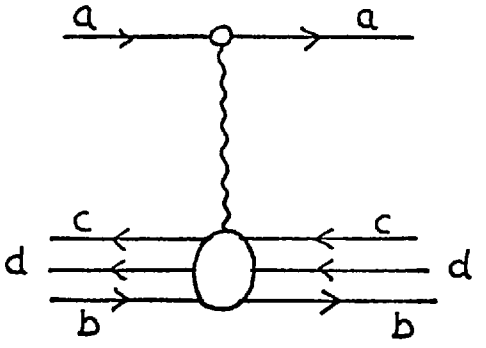

e

Fig. 6

Then also

$$X^2 = (1-\alpha_1-\alpha_2)(1-\beta_1-\beta_2)\,s \;\to\; s$$

Therefore to obtain the multi-Regge configuration of Fig. 6a we have the additional constraints

$$s \to X^2 \quad , \qquad s_{ac}\, s_{cd}\, s_{db}/s \;\to\; \text{constant}$$

On the basis of the multi-Regge model with a factorizable Regge pole we would expect the 4→4 amplitude to be given by

$$(s_{ac}\, s_{cd}\, s_{db})^{\alpha_V(0)} G_a . G_b . F(\underline{K}_1^2)\, F(\underline{K}_2^2) \qquad 2.29$$

where $\alpha_V(0)$ is the intercept of the Pomeron, G_a is the coupling of particle a to the Pomeron, and $F(\underline{K}^2)$ is the two Pomeron-two particle coupling 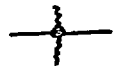 . What we actually need is the discontinuity of this amplitude in the variable X^2. Using field theory models (28) it has been shown that this discontinuity indeed results in the factorized form

$$(s_{ac}\, s_{cd}\, s_{db})^{\alpha_V(0)} g_a\, g_b\, f(\underline{K}_1^2)\, f(\underline{K}_2^2) \qquad 2.30$$

We will discuss one of these model proofs in Chapter III, So, while in general some dependence on $\underline{K}_1 . \underline{K}_2$ is expected, it turns out that in this case it is suppressed.

If we now replace . $s_{ac}\, s_{cd}\, s_{db}$ by $(1-\underline{K}_1^2)(1-\underline{K}_2^2)\,s$ we get

$$F \sim s^{\alpha_V(0)-1} . g_a\, g_b . g(\underline{K}_1^2) . g(\underline{K}_2^2) \qquad 2.31$$

where $g(\underline{K}_1^2) = f(\underline{K}_1^2) . (1-\underline{K}_1^2)^{\alpha_V(0)}$

If $\alpha_V(0) = 1$ therefore, we have Feynman scaling i.e. the cross-section is independent of s. If $\alpha_V(0)$ is not exactly 1 we may divide by the ab total cross-section $g_a g_b\, s^{\alpha_V(0)-1}$ and we obtain

a distribution which does scale. The function $g(\underline{K}^2)$ is the same function which appears in the single particle inclusive cross-section in the pionization region. Since the Feynman variable $x = \alpha - \beta$, both particles c and d are in the pionization region with x= 0.

Le Bellac (29) has shown that it is not consistent to have the Pomeron dominating the total cross-section and the 3→3 and 4→4 amplitudes if its intercept is exactly 1, and if it is factorizable with no zeros in the two Pomeron-two particle vertex function. Presumably this is connected in some way with the Finkelstein-Kajantie (30) disease of standard multi-Regge theory to which the usual solution is to take the Pomeron intercept at some value just below 1. This also overcomes Le Bellac's objections.

b) Fig. 6b represents the region

$$s_{ac} \to -\infty \quad , \qquad s_{cd} \to \infty \quad ,$$

$$s_{db} \qquad \text{fixed small,}$$

such that $s_{ac}.s_{cd}/s$ is fixed and small and

s/x^2 is fixed and small.

This last condition ensures that none of the combinations α_1, $\alpha_1+\alpha_2$, β_2, $\beta_1+\beta_2$ approach 1. If this were so the diagrams discussed in sections 1 and 3 would be more appropriate, in which the particle (s) c or d or c + d take(s) away virtually all the momentum of a or b giving a leading particle effect.

The present limit corresponds to single fragmentation of b (giving d) and the production of a pionized particle c .

We expect the factorised form

$$F \sim \frac{1}{s} (s_{ac} s_{cd})^{\alpha_v(0)} f(\underline{K}_1^2).\bar{f}(\underline{K}_2^2, s_{db}).g_a \qquad (2.32)$$

$$S_{ac} = -\beta_1 S \quad ,$$

$$S_{cd} = (\alpha_1\beta_2 + \alpha_2\beta_1)S \quad \text{both} \quad \to \infty \tag{2.33}$$

We therefore demand as before that $\alpha_1 >> \alpha_2$, with $\alpha_1 \sim O\left(\frac{1}{S^n}\right)$, $0<n<1$. This gives

$$S_{ac}\, S_{cd} \sim -\beta_1 S \alpha_1 \beta_2 S = -(1-\underline{K}_1^2)\beta_2 S \tag{2.34}$$

since $S_{db} = -\alpha_2 S + \underline{K}_2^2$ is small, $\alpha_2 \sim O(1/S)$ and $\beta_2 \sim$ constant giving $S_{ac}.S_{cd}/S$ is fixed and small (equal to some function of $\underline{K}_2^2$ and S_{db}), so again we have scaling in s.

$$F \sim s^{\alpha_V(0)-1} \cdot g_a \cdot g(\underline{K}_1^2) \cdot \bar{g}(\underline{K}_2^2, S_{db}) \tag{2.35}$$

c) Fig. 6c represents

$$S_{ac} \to -\infty \quad , \qquad S_{db} \to -\infty \quad ,$$

$$S_{cd} \quad \text{fixed small}$$

such that $S_{ac}S_{db}/S$ and S/X^2 are fixed and small. Here two particles are produced in the pionization region with approximately equal energy. In terms of Sudakov variables this means $\alpha_1 \gtrsim \alpha_2$ and $\beta_1 \lesssim \beta_2$. Then

$$F \sim \frac{1}{S}\left(S_{ac}\, S_{bd}\right)^{\alpha_V(0)} \cdot g_a g_b f_2(S_{cd}, \underline{K}_1^2, \underline{K}_2^2, \underline{K}_1.\underline{K}_2) \tag{2.36}$$

We now expect some dependence on $\underline{K}_1.\underline{K}_2$ unless the particles are produced in a completely uncorrelated fashion. We postpone discussion of this point until Chapter IV.

Now $S_{ac}\, S_{bd} = \alpha_2\beta_1 S^2 = \frac{\alpha_2}{\alpha_1}(1-\underline{K}_1^2)S$

but $s_{cd} = (\alpha_1\beta_2 + \beta_1\alpha_2)s + (\underline{K}_1+\underline{K}_2)^2 =$

$$\frac{\alpha_1}{\alpha_2}(1-\underline{K}_2^2) + \frac{\alpha_2}{\alpha_1}(1-\underline{K}_1^2) + (\underline{K}_1+\underline{K}_2)^2 \qquad (2.37)$$

is small.

Consequently α_2/α_1 is fixed in terms of $\underline{K}_1^2$, $\underline{K}_2^2$, $\underline{K}_1.\underline{K}_2$ and s_{cd} and

$$F \sim g_a g_b \cdot g_2(s_{cd}, \underline{K}_1^2, \underline{K}_2^2, \underline{K}_1.\underline{K}_2)\, s^{\alpha_V(0)-1} \qquad (2.38)$$

d) Fig. 6d represents

$$s_{ac} \quad \text{fixed small}, \qquad s_{db} \quad \text{fixed small}$$

$$s_{cd} \to \infty$$

such that s_{cd}/s and s/x^2 are fixed and small.

This limit corresponds to fragmentation of a into c and b into d. Since these occur at opposite ends of the Reggeon we would expect the momenta of c and d to be uncorrelated and in fact we expect F to be equal to the product of two single particle inclusive cross-sections in the fragmentation limit divided by the total cross section.

$$F \sim \left(\frac{s_{cd}}{s}\right)^{\alpha_V(0)} \cdot \bar{f}(s_{ac}, \underline{K}_1^2)\, \bar{f}(s_{bd}, \underline{K}_2^2) \qquad (2.39)$$

but $s_{cd} \sim \alpha_1\beta_2 s$ and since s_{ac} and s_{bd} are fixed small this implies α_1 and $\beta_2 \sim$ constant (<1), and again we have

$$F \sim s^{\alpha_V(0)-1}\, \bar{g}(s_{ac}, \underline{K}_1^2)\, \bar{g}(s_{bd}, \underline{K}_2^2) \qquad (2.40)$$

where $\bar{g}(s_{ac}, \underline{K}_1^2)$ is the fragmentation cross section of a into c, divided by g_b, and similarly for $\bar{g}(s_{bd}, \underline{K}_2^2)$.

Freedman, et. al. (31) have also investigated this particular configuration and show that there is no $\underline{K}_1 . \underline{K}_2$ dependence if the Pomeron is a simple pole.

e) Figure 6e describes the region

$$s_{ac} \to -\infty \quad , \qquad s_{cd} \quad \text{fixed small} \, ,$$

$$s_{db} \quad \text{fixed small},$$

such that s_{ac}/s and s/χ^2 are fixed small.

This is double fragmentation of b.

$$F \sim \frac{1}{s} (s_{ac})^{\alpha_v(0)} \cdot f_3(s_{ac}, s_{db}, \underline{K}_1^2, \underline{K}_2^2, \underline{K}_1 . \underline{K}_2) . g_a \qquad (2.41)$$

$s_{ac} \sim -\beta_1 s$. Since s_{db} and s_{cd} are small $\alpha_1 \sim \alpha_2 \sim O(\frac{1}{s})$ giving $\beta_1 \sim$ constant. Then

$$F \sim s^{\alpha_v(0)-1} \cdot g_a \cdot g_3(s_{ac}, s_{bd}, \underline{K}_1^2, \underline{K}_2^2, \underline{K}_1 . \underline{K}_2) \qquad (2.42)$$

Scaling in s is a common feature of all the five limits discussed in this section. If $\alpha_v(0) = 1$ the cross-section scales. If $\alpha_v(0) \neq 1$ the cross-section divided by the ab total cross-section scales.

In all cases s/χ^2 is finite. If however χ^2 goes infinite together with s/χ^2 we have another interesting limiting case.

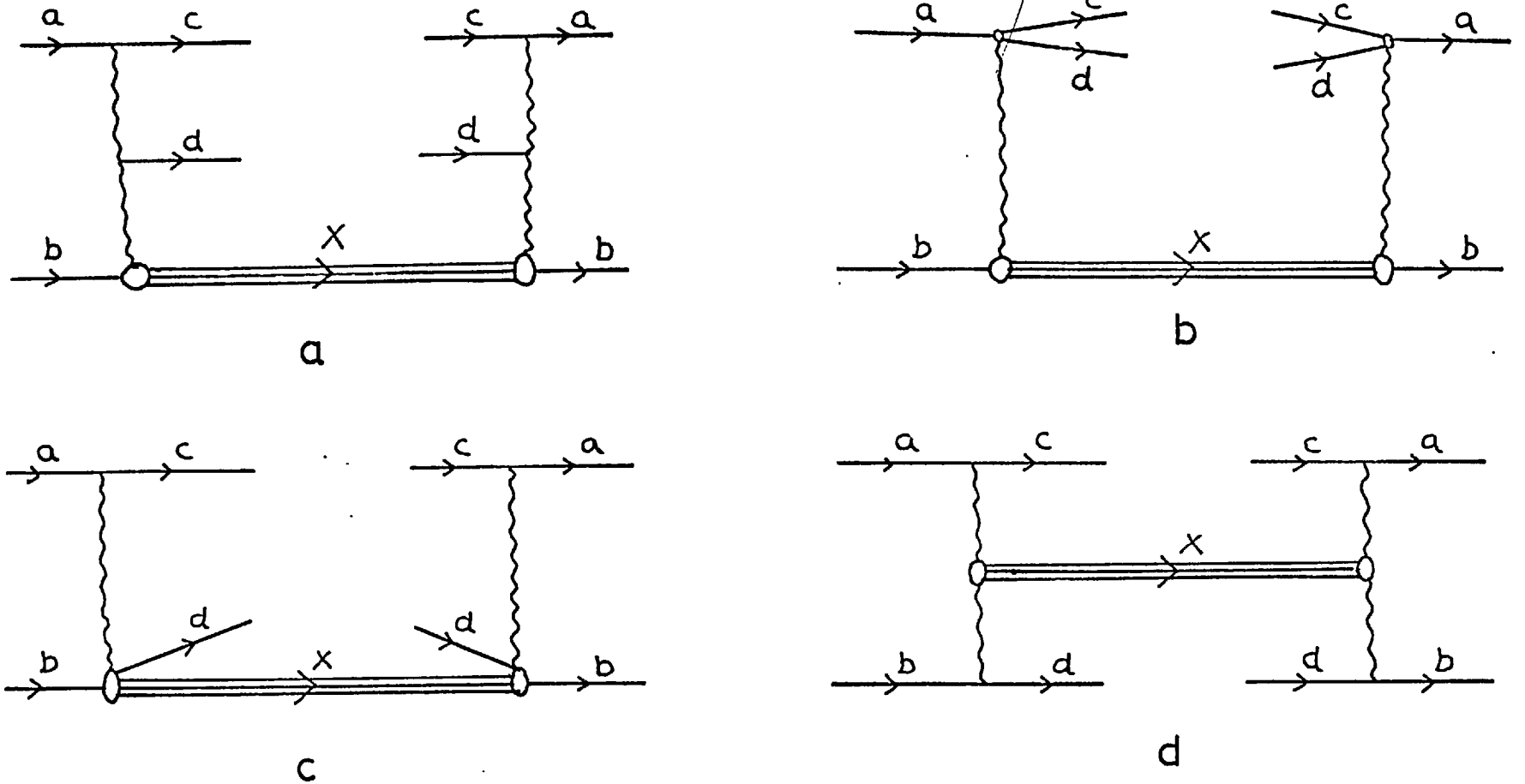

Fig. 7

3) When s/X^2 and $X^2 \to \infty$ either

$$1 - \alpha_1 - \alpha_2 \sim O\left(\frac{1}{s^n}\right), \quad 0 < n < 1,$$

or $$1 - \beta_1 - \beta_2 \sim O\left(\frac{1}{s^n}\right). \tag{2.43}$$

Consequently we are led to using Figs. 7 a $\to$ d to represent this region of phase space, since these conditions mean that one or other or both of these particles carry off most of the momentum of one of the incoming particles. We discuss this region in terms of the multi-Regge model for $2 \to n$ processes.

a) Fig. 7a represents the region

s_{ac} fixed small, $s_{cd} \to \infty$

s_{acd} fixed small, $s_{bac} \to \infty$,

such that $\frac{s_{cd}\, s_{bac}}{s}$ is finite and $\frac{s}{X^2} \to \infty$, and $\frac{s_{bac}}{X^2} \to \infty$

Consider the amplitude represented by Fig. 8a. Multi-Regge

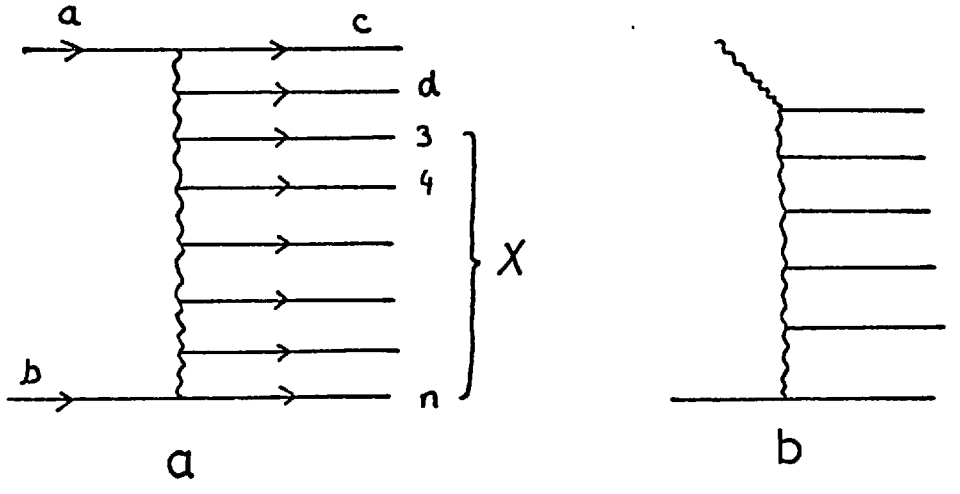

Fig. 8

kinematics are such that $\alpha_1 >> \alpha_2 >> \cdots >> \alpha_n$ with $\alpha_1 \to 1$, $\alpha_n \sim O(1/s)$. It is also a property of this region of phase space that (25)

$$\frac{s_{cd}\, s_{d3} \cdots s_{n-1\,n}}{s} = \prod_{i=2}^{n-1} (1-\underline{k}_i^2) \qquad 2.44$$

Then the amplitude of Fig. 8a is

$$s_{cd}^{\alpha(s_{ac})} \left[\frac{s}{x^2 s_{cd}}\right]^{\alpha(s_{acd})} \cdot A \cdot [1-\underline{k}_2^2]^{\alpha(s_{acd})} \times$$

$$g_c(s_{ac}) \cdot g_d(s_{ac}, s_{acd}, s_{cd}\, s_{acb}/s) \qquad 2.45$$

where A is the amplitude of Fig. 8b . $\alpha(s_{ac})$ is the leading Regge trajectory coupling to the system with the quantum numbers of $a\bar{c}$ etc., and g_d is the coupling of d to two Reggeons(and includes signature factors).

If we then put two of these diagrams back to back, to calculate the cross-section we get

$$F \sim s_{cd}^{2\alpha(s_{ac})} \cdot \left[\frac{s}{x^2 \cdot s_{cd}}\right]^{2\alpha(s_{acd})} \cdot g_c^2(s_{ac}) \times$$

$$g_d^2(s_{ac}, s_{acd}, s_{cd}\, s_{acb}/s) \cdot [1-\underline{k}_2^2]^{2\alpha(s_{acd})} \cdot \sum_{x^2} AA^+ \qquad 2.46$$

From unitarity we expect that $\sum_{x^2} AA^+$ generates the imaginary part of the Reggeon-particle forward amplitude (25,32) given by $(x^2)^{\alpha_V(0)} g_b\, f_{PRR}(s_{acd})$ where g_b is the coupling of the Pomeron to b, and $f_{PRR}(s_{acd})$ is the Regge-Regge-Pomeron coupling (33). (Fig. 9)

Thus we expect

$$F \sim s^{2\alpha(s_{acd})-1} \cdot s_{cd}^{2\alpha(s_{ac})-2\alpha(s_{acd})} \cdot (x^2)^{\alpha_V(0)-2\alpha(s_{acd})} \times \qquad 2.47$$

$$f_{PRR}(s_{acd})\, f_c^2(s_{ac})\, f_d^2\left(s_{ac}, s_{acd}, \frac{s_{cd}\, s_{acb}}{s}\right) \cdot g_b$$

where $(1-\underline{K}_2^2)^{2\alpha(S_{acd})}$ has been absorbed into g_d^2 to give f_d^2 .
($\underline{K}_2^2$ can be expressed in terms of S_{ac} , S_{acd} and $\frac{S_{cd}\,S_{acb}}{S}$)

Fig. 9

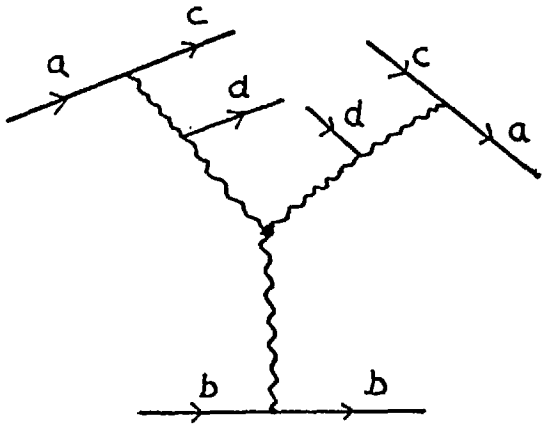

b) Fig, 7b represents

S_{ac} fixed small, S_{cd} fixed small,

$S_{bac} \to \infty$, S_{acd} fixed small,

such that $\frac{S_{bac}}{S}$ is finite, $\frac{S_{bac}}{X^2} \to \infty$

Asimilar analysis to the above gives

$$F \sim \frac{1}{S} \cdot S_{bac}^{2\alpha(S_{acd})} \cdot (X^2)^{\alpha_v(0)-2\alpha(S_{acd})} \times \qquad 2.48$$

$$f_{PRR}(S_{acd}) \cdot g_b \cdot f_a^2 (S_{ac}, S_{acd}, S_{bac}/S)$$

c) This region is not very interesting as the information that can be gained , can also be obtained from single particle inclusive experiments.

d) Fig. 7d describes

S_{ac} fixed small, S_{bd} fixed small,

$S_{bac} \to \infty$, $S_{bad} \to \infty$.

such that $S/S_{bac} \to \infty$, $S/S_{bad} \to \infty$,

and $\frac{S_{bac}\, S_{bad}}{X^2\, s}$ is finite.

These last conditions ensure that we have the correct multi-Regge kinematics for digram 7d.

$$F \sim \frac{1}{s}\left(\frac{s}{s_{bac}}\right)^{2\alpha(s_{ac})} \cdot \left(\frac{s}{s_{bad}}\right)^{2\alpha(s_{bd})} \cdot (X^2)^{2\alpha_V(0)} \times$$

$$g_c(s_{ac}) \cdot g_d(s_{bd}) \cdot f_{PRR}(s_{ac}) \cdot f_{PRR}(s_{bd}) \qquad 2.49$$

This is the so-called di-triple-Regge limit (Fig.10).

Fig. 10

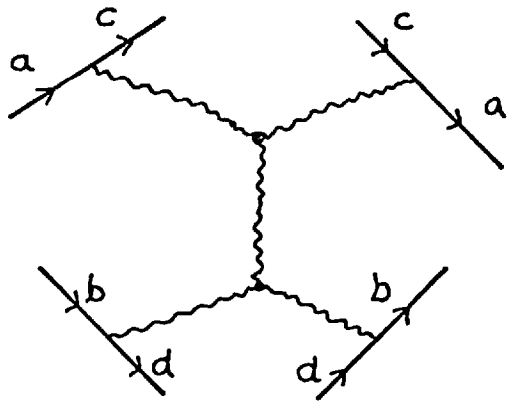

2.4 Discussion

The two particle inclusive distributions have also been studied by Abarbanel (34) and Jen et al (35). Where the predictions overlap, agreement is obtained. Abarbanel uses SO(1,3) expansions to discuss the limits discussed in sub-section 2, and in particular considers the effect of the lower lying P' trajectory on how rapidly the scaling limit is approached. Both our approach and Abarbanel's suffer from the fact that we can make no predictions on the form of the residue functions. Jen et al, on the other hand, use the generalized Veneziano model which is completely specified and therefore they can obtain an explicit prediction for the residue

function in all the different limits. For example, they obtain, for the two Pomeron-two particle coupling,a function which decreases rapidly to zero as $\underline{K}^2$ gets large, agreeing with experimental observation. However the standard dual model they use does not incorporate the Pomeron, which is the most important trajectory in Mueller's approach. So while this approach may be useful as a guide to the sort of functions one might expect, we feel that any specific predictions are not to be trusted.

We have neglected Regge cuts throughout this discussion. this is perhaps a more serious omission in sub-sections 1) and 3) than it is in 2). In the latter case all the momentum transfers associated with the Pomeron are zero, so we are concerned with the intercepts of trajectories only. If the Pomeron pole is at 1 at t=0, then so is the Pomeron-Pomeron cut. However cut contributions to the amplitude die away as inverse powers of log(s) compared with pole contributions, thus at high enough energies the cut contributions should be negligible.(unless there are an infinite number of cuts as suggested by the eikonal picture (36)). If, as suggested by multiperipheral calculations (30) the Pomeron intercept is just below 1 at $1-\epsilon$, the cut intercept is at $1-2\epsilon$ and the cut contributions die away more rapidly with increasing energy than when the pole intercept is at 1. This would also improve the situation in sub-sections 1) and 3) where the Pomeron-Regge cut will still be below the pole for asmall range of momentum transfer. However as the momentum transfers increase the cuts will become dominant. If cuts are important, as they appear to be in two-body reactions, then not only will there be additional terms depending on log(s) ,but we will not be able to make the assumptions that we have made concerning the

factorization of the multi-Regge amplitudes.

CHAPTER III

FACTORIZATION OF THE TWO PARTICLE INCLUSIVE CROSS-SECTION

3.1 Introduction

In Chapter II we predicted the behaviour of the two particle inclusive cross-sections in the pionization and fragmentation regions (2.3 sub-section 2) on the assumption that when particles c and d were separated by a Reggeon, the discontinuity of the 4→4 amplitude in the X^2 variable factorized. Intuitively this is appealing , since no momentum is transferred down the Reggeon and therefore we might expect no $\underline{K}_1.\underline{K}_2$ dependence. We investigate this using a field theory model due to Gribov (37). The model essentially replaces infinite sums of graphs by complete off-mass-shell amplitudes. The assumption is then made that the dominant contribution to the asymptotic behaviour of the whole amplitude is given by the model when the masses of the off-mass-shell particles remain finite. This model has been used by Drummond (38) and Campbell (39) to discuss multi-Regge amplitudes, and in the realm of inclusive reactions Botke (40) has used it to investigate multi-Reggeon effects.

We want then to show that, if the single particle inclusive cross-section in the pionization region (Fig. 1a) is given by

$$s^{\alpha_V(0)-1} \cdot g_a g_b f(\underline{K}^2)$$ then the two particle inclusive cross-section of Fig. 1b is given by

$$s^{\alpha_V(0)-1} \cdot g_a g_b f(\underline{K}_1^2) f(\underline{K}_2^2)$$

3.2 The Cross-sections

a) The two-particle inclusive cross-section.

To evaluate this we calculate the discontinuity of the Feynman

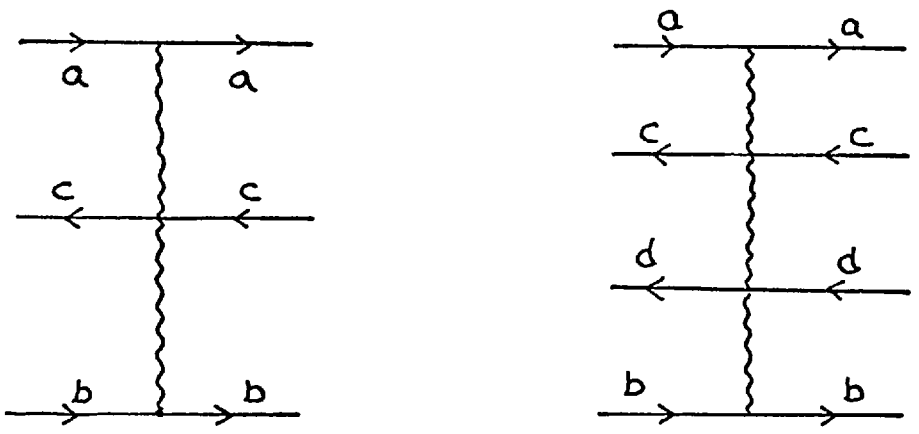

a Fig. 1 b

diagram of Fig. 2 in the variable $X^2=(a+b-c-d)^2$ we must therefore replace the amplitudes A_1,A_2 and A_3 by the discontinuities of the amplitude A_1 in the variable s_1, A_2 in s_2, and A_3 in s_3 respectively. This is because, to get the appropriate discontinuity, we must cut the diagram along the dotted line as in Fig. 2 to get T on the left and T^* on the right, where T is the amplitude $a+b+\bar{c}+\bar{d}\rightarrow$ anything. Since this line must therefore not cut any of the propagators it must cut each 'blob'. Thus each blob becomes an integral over AA^* which by elastic unitarity is the discontinuity of A in the relevant energy variable. If the internal particles all have mass m, we get a non-zero contribution only when all the $s_i>4m^2$ (i=1,2,3). We shall, in all that follows, put all internal and external masses equal to 1.

As in Chapter II we define the Sudakov variables and denote

$$a\sim(1,0,0)\quad,\quad b\sim(0,1,0),$$
$$c=(\alpha_1,\beta_1,\underline{K}_1)\quad,\quad d=(\alpha_2,\beta_2,\underline{K}_2),$$
$$q_1=(\gamma_1,\delta_1,\underline{Q}_1)\quad,\quad q_2=(\gamma_2,\delta_2,\underline{Q}_2) \qquad 3.1$$

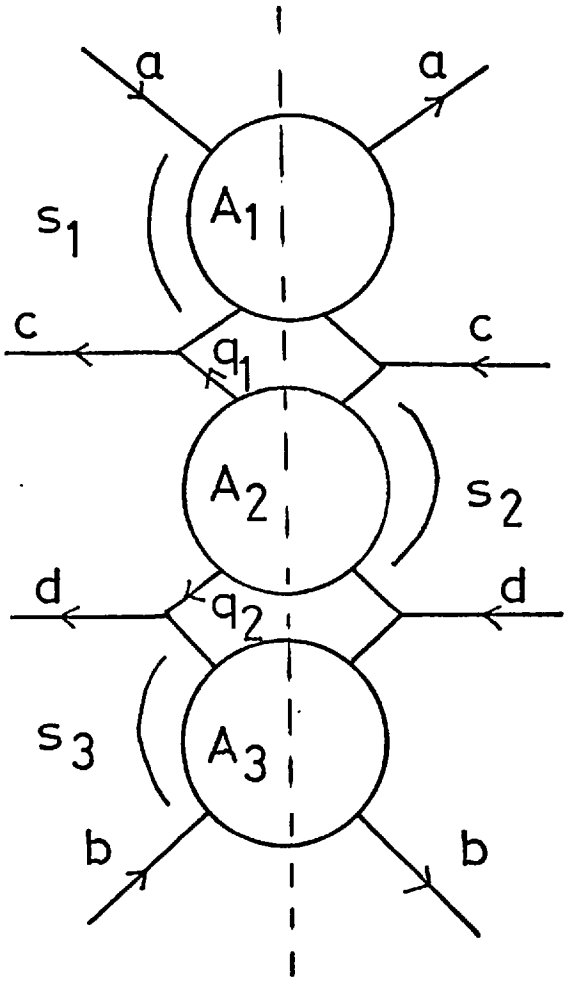

Fig. 2

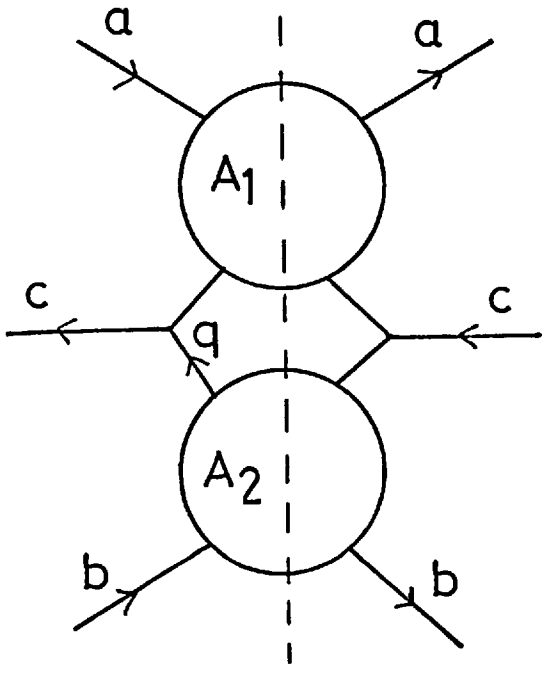

Fig. 3

then as $s \to \infty$

$$S_1 = (\delta_1 - \beta_1)s + (\underline{Q}_1 - \underline{K}_1)^2$$

$$S_2 = (\gamma_1\delta_2 + \gamma_2\delta_1)s + (\underline{Q}_1 + \underline{Q}_2)^2$$

$$S_3 = (\gamma_2 - \alpha_2)s + (\underline{Q}_2 - \underline{K}_2)^2 \qquad 3.2$$

Following Drummond (38) and Campbell (39) we scale the γ_i and δ_i thus

$$\delta_1 s = s_{ac} Y_1 \Rightarrow S_1 = s_{ac}(1+Y_1) + (\underline{Q}_1 - \underline{K}_1)^2$$

$$\gamma_2 s = s_{bd} Y_2 \Rightarrow S_3 = s_{bd}(1+Y_2) + (\underline{Q}_2 - \underline{K}_2)^2 \qquad 3.3$$

and $\quad X_1 = \gamma_1 s_{ac}, \quad X_2 = \delta_2 s_{bd}$

so that

$$S_2 = \frac{X_1 X_2 s}{s_{ac} s_{bd}} + Y_1 Y_2 \frac{s_{bd} s_{ac}}{s} + (\underline{Q}_1 + \underline{Q}_2)^2 \qquad 3.4$$

In the region where s_{ac}, s_{bd}, and s_{cd} are all infinite,

$$s_{ac} s_{bd} s_{cd} = (1-\underline{K}_1^2)(1-\underline{K}_2^2)s$$

and we have $S_2 \sim X_1 X_2 s_{cd}/\eta$ where $\eta = (1-\underline{K}_1^2)(1-\underline{K}_2^2)$

unless both X_1 and X_2 are $\sim O\left(\frac{1}{s_{cd}}\right)$ or Y_1 and Y_2 are infinite. This latter case can be ruled out as this would mean that the propagator momenta squared would become infinite. We assume that for these propagators to be finite, we require X_i, Y_i, $\underline{Q}_i^2$ to be finite. We will return to this point later. With this assumption, the major contributions to the diagram come from the region where s_1, s_2 and s_3 all $\to \infty$. We can therefore use the Regge pole form for the discontinuities which gives us $\quad Disc_{X^2} A =$

$$\int \prod_{i=1}^{2} d^4 q_i \; (s_1 s_2 s_3)^{\alpha_V(0)} \left[\frac{1}{(q_1^2 - 1)} \cdot \frac{1}{(q_2^2 - 1)} \cdot \right.$$

$$\left. \cdot \frac{1}{(q_1 - c)^2 - 1} \cdot \frac{1}{(q_2 - d)^2 - 1} \right]^2 \cdot g_1 \cdot g_2 \cdot f(q_1^2) \cdot f(q_2^2) \cdot \qquad 3.5$$

$$\cdot f((q_1 - c)^2) \cdot f((q_2 - d)^2)$$

We have kept only the leading Regge singularity, i.e. the Pomeron, and have assumed that is a simple pole with intercept $\alpha_V(0)$ with a factorized residue. The discontinuity of the forward $2\to2$ amplitude is thus also factorized. g_1 is the coupling of the Pomeron to a, g_2 the coupling of the Pomeron to b, $f(q_i^2)$ the coupling of the Pomeron to the propagators whose four-momenta are q_1, etc.

Changing to Sudakov variables we get $\mathrm{Disc}_{X^2} A =$

$$\left(\frac{1}{2}|S|\right)^2 \int \prod_{i=1}^{2} (d\gamma_i d\delta_i d^2Q_i) \cdot ((\delta_1-\beta_1)s \cdot (\gamma_1\delta_2+\delta_1\gamma_2)s \times$$

$$\cdot(\gamma_2-\alpha_2)s)^{\alpha_V(0)} \cdot \prod_{i=1}^{2} \left[\frac{1}{(\gamma_i\delta_i s+\underline{Q}_i^2-1)} \cdot \frac{1}{((\beta_i-\delta_i)(\alpha_i-\gamma_i)s+(\underline{Q}_i-\underline{K}_i)^2-1}\right]^2 \times$$

$$\cdot g_1 g_2 \prod_{i=1}^{2} f((\beta_i-\delta_i)(\alpha_i-\gamma_i)s+(\underline{Q}_i-\underline{K}_i)^2) \cdot f(\gamma_i\delta_i s+\underline{Q}_i^2) \cdot$$

3.6

We now want to change the variables γ_i, δ_i to X_i, Y_i. We need to know the range of integration of the X_i and Y_i.

Since s_1, s_2, s_3 must $> 4(m^2)$ to give any contribution we have

$$\begin{aligned} s_{ac}(1+Y_1) &> 4-(\underline{Q}_1-\underline{K}_1)^2, \\ s_{bd}(1+Y_2) &> 4-(\underline{Q}_2-\underline{K}_2)^2, \\ s_{cd}\eta^{-1}X_1X_2 &> 4-(\underline{Q}_1+\underline{Q}_2)^2 \end{aligned} \qquad 3.7$$

Now $\underline{Q}$ and $\underline{K}$ are space-like vectors, and moreover both have finite norm so the right hand sides are all finite positive numbers.

s_{ac} and s_{bd} are large and negative, so $1+Y_1$ and $1+Y_2$ are negative such that

$$1+Y_1 < -\frac{(4-(\underline{Q}_1-\underline{K}_1)^2)}{|s_{ac}|}, \quad 1+Y_2 < -\frac{(4-(\underline{Q}_2-\underline{K}_2)^2)}{|s_{bd}|}$$

As $|s_{ac}|$ and $|s_{bd}| \to \infty$ this implies

$$\gamma_1 < -1 \ , \quad \gamma_2 < -1 \qquad 3.8$$

s_{cd} is positive and $\to \infty$ so similarly $X_1 X_2 > 0$. So we can have either both X_1 and X_2 positive or both negative.

From elastic unitarity, the energy flowing through each blob from left to right must be positive. This gives us the conditions

$$\begin{aligned} &1 + \gamma_1 + \delta_1 - \alpha_1 - \beta_1 > 0 \ , \\ &1 + \gamma_2 + \delta_2 - \alpha_2 - \beta_2 > 0 \ , \\ &\gamma_1 + \gamma_2 + \delta_1 + \delta_2 < 0 \end{aligned} \qquad 3.9$$

(The energy of particle $(\alpha, \beta, \underline{k})$ in the centre of mass frame of a and b is $(\alpha+\beta)\sqrt{s}/2$.)

Now δ_1 and γ_2 are positive, from the positivity conditions on s_1 and s_3, so

$$\gamma_1 + \delta_2 < -(\gamma_2 + \delta_1) \qquad 3.10$$

Since X_1 and X_2 both have the same sign, so do γ_1 and δ_2 . This must , from the above condition, be negative. This condition is automatically satisfied if X_1 and X_2 are greater than $O(1/s_{cd})$ as can be seen from the definitions

$$|\gamma_1| = \left| \frac{X_1}{s_{ac}} \right| > |\gamma_2| = \left| \frac{\gamma_2 \eta}{s_{ac} s_{cd}} \right| \qquad \text{unless } X_1 \sim O\left(\frac{1}{s_{cd}}\right)$$

$$|\delta_2| = \left| \frac{X_2}{s_{bd}} \right| > |\delta_1| = \left| \frac{\gamma_1 \eta}{s_{bd} s_{cd}} \right| \qquad \text{unless } X_2 \sim O\left(\frac{1}{s_{cd}}\right) \qquad 3.11$$

assuming γ_1 and γ_2 remain finite. If either γ_1 or γ_2 go infinite the integrand vanishes due to the off-mass-shell effects and if X_1 or X_2 become so small that the condition 3.10 fails, the integrand will be negligible due to the $(X_1 X_2)^{\alpha_V(0)}$ term in the numerator (see below). Therefore X_1 and X_2 are both positive with lower limits $\to 0$,and upper limits fixed in terms of the γ_i by the

conditions 3.9. These in fact allow $X_i \to O(s_{cd})$ so we take

$$-\infty < Y_i < -1 \ ,$$

$$\infty > X_i > 0 \ .$$

Thus we have $\mathrm{Disc}_{X^2} A \sim$

$$\frac{1}{4} |s_{ac}|^{\alpha_V} (s_{cd}/\eta)^{\alpha_V} |s_{bd}|^{\alpha_V} \int \prod_{i=1}^{2} \Big[dX_i\, dY_i\, d^2\underline{Q}_i \times$$

$$\Big[\frac{1}{(X_i Y_i + \underline{Q}_i^2 - 1)} \cdot \frac{1}{(X_i Y_i + \eta_i Y_i + X_i + \alpha_i\beta_i s + (\underline{Q}_i - \underline{K}_i)^2 - 1)} \Big]^2 \cdot \Theta(X_i) \times$$

$$\Theta(-1-Y_i) \Big] \cdot |1+Y_1|^{\alpha_V} |1+Y_2|^{\alpha_V} \cdot |X_1 X_2|^{\alpha_V} \cdot f(q_i^2) \times$$

$$f(q_i^2) \cdot f((q_1-c)^2) \cdot f((q_2-d)^2) \cdot g_1 g_2$$

3.12

where $(q_1-c)^2 = X_1 Y_1 + \eta_1 Y_1 + X_1 + \alpha_1\beta_1 s + (\underline{Q}_1 - \underline{K}_1)^2$

etc. neglecting terms to order $1/s_{cd}$ and $\eta_1 = 1 - \underline{K}_1^2$

Note that $s_{ac}\, s_{cd}\, s_{bd} \sim \eta\, s$ in this region.

In this form it can be seen that the discontinuity factorizes, since the region of integration is factorized as well as the integrand.

b) The single particle inclusive cross-section.

If the same calculation is performed for the 3→3 amplitude (Fig. 3) we get $\mathrm{Disc}_{X^2} A \sim$

$$\frac{1}{2} g_1 g_2 \int dX\, dY\, d^2Q \ \frac{|s_{ac}|^{\alpha_V} |s_{cb}|^{\alpha_V}}{\eta^{\alpha_V}} \cdot |1+Y|^{\alpha_V} |X|^{\alpha_V} \times$$

$$\Theta(X)\Theta(-1-Y) \cdot \Big[\frac{1}{(XY + \underline{Q}^2 - 1)} \cdot \frac{1}{(XY + \eta Y + X + \alpha\beta s + (Q-K)^2 - 1)} \Big]^2 \times$$

$$f(q^2) \cdot f((q-c)^2) \cdot$$

3.13

where $X = \gamma s_{ac}$, $Y = s s / s_{ac}$,

$$\eta = 1 - \underline{K}^2 \qquad 3.14$$

and $q_y^2 = XY + \underline{Q}^2$ etc.

with $s_{ac}\, s_{cb} \sim \eta s$.

The limits of integration are $-\infty < Y < -1$,

and $X > 0$ with its upper limit fixed in terms of Y by the condition $1 + \gamma + \delta - \alpha - \beta > 0$.

The range of integration is therefore the same in the 3→3 case as in the two separate integrals in the 4→4 case.

We have thus demonstrated the required factorization of the leading order contribution to the two particle spectrum in the double pionization region, since if the single particle inclusive cross-section is $g_1 g_2 s^{\alpha_v - 1} g(\underline{K}^2)$ the two particle inclusive cross-section is $g_1 g_2 s^{\alpha_v - 1} g(\underline{K}_1^2)\, g(\underline{K}_2^2)$.

Now let us return to the question of the finiteness of the parameters X, Y and $\underline{Q}^2$. We will use the 3→3 case, as the n→n case is merely a product of n-2 identical pieces. The 'masses' of the propagators are

$$\begin{aligned} &1 \qquad XY + \underline{Q}^2 \\ &2 \qquad XY + \eta Y + X + \alpha\beta s + (\underline{Q} - \underline{K})^2 \end{aligned} \qquad 3.15$$

$\underline{Q}^2$ and $(\underline{Q} - \underline{K})^2$ are negative since these are spacelike vectors, Y is negative from the condition $s_1 > 4$, and X is positive from the condition $s_2 > 4$. Therefore XY and $\underline{Q}^2$ are finite from condition 3.15-1 . $\underline{K}^2$ is always finite, therefore so is $(\underline{Q} - \underline{K})^2$ Together with 3.15-2 these show that neither X nor Y can go infinite if the 'masses' are to remain finite.

Factorization has also been demonstrated in φ^3 field theory using the ladder diagrams Fig. 4 (28). The amplitudes

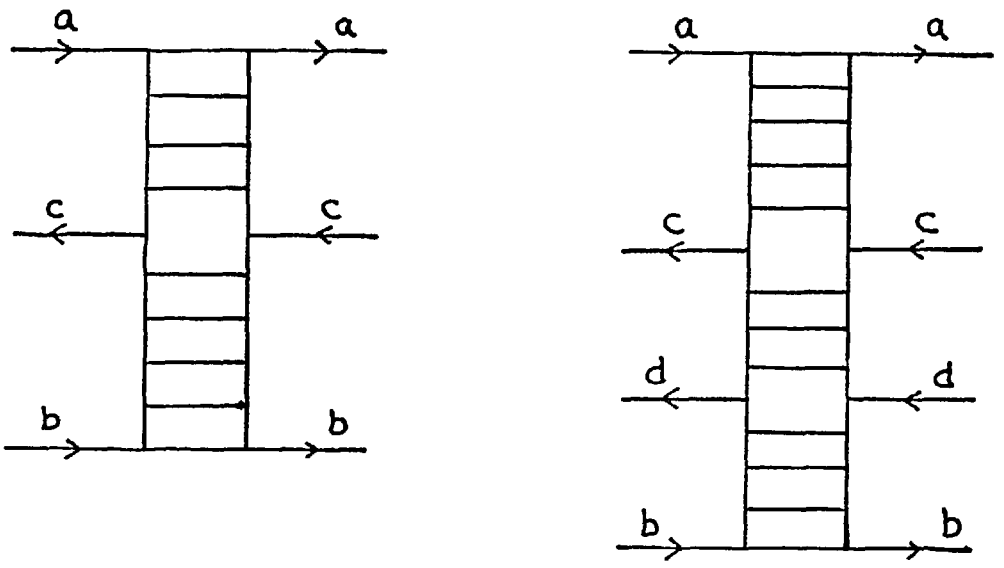

Fig. 4

generated by the graphs are calculated, then the continuation is performed around the X^2 cut from $X^2+i\epsilon$ to $X^2-i\epsilon$,keeping all the other variables fixed with respect to their cuts, and the discontinuity is calculated directly. Weis (41) and Jen et al (35) have proved this factorization in the Veneziano model.

CHAPTER IV

THE DISTRIBUTION OF PRODUCED PARTICLES

4.1 Introduction

Mueller (7) has shown that, for a theory which scales in the sense defined by Feynman (1) or Benecke et al (2) , the multiplicity of produced particles $\bar{n}(s) \xrightarrow[s\to\infty]{} a \log s + b$, where the logarithmic increase may be attributed to pionization particles or fast (defined in the rest frame of the particle which fragments) fragments of the target and projectile, according to which picture one prefers. He shows how $\bar{n}$ may be calculated from the single particle inclusive cross-section,

$$\bar{n} = \frac{1}{\sigma(s)} \int \frac{d^3p}{E} \left(\frac{d\sigma}{d^3p} . E \right) \qquad 4.1$$

where $\sigma(s)$ is the total cross-section for the beam particle on the target particle. Here $\bar{n}$ refers to the specific type of particle observed e.g. π^-, π^+ . This is because an inclusive reaction includes many exclusive reactions i.e. $p+p \to \pi^+ + X$ includes $p+p \to p + n + \pi^+ + \pi^+ + \pi^-$ say, and in this case the observed pion may be one of two. Thus in the inclusive cross-section the contribution of the cross-section for producing n of the type of particle observed is weighted by n, since all configurations contribute. The mean multiplicity is then given by the diagramatic equation

$$\bar{n} = \frac{1}{\sigma(s)} \int \frac{d^3p}{E} \Big[$$

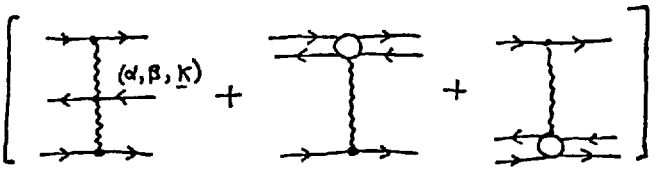

$$\Big] \qquad 4.2$$

i ii iii

where the diagrams represents $E\,\frac{d\sigma}{d^3p}$ in the relevant region of phase space. The regions of phase space where X^2 is small or s/X^2 and X^2 both $\to \infty$ have been neglected, (12) because they correspond to an infinitessimal volume as shown below

$$X^2 = (1-\alpha)(1-\beta)s + \underline{K}^2 \qquad 4.3$$

so X^2 small means $1-\alpha \sim O(\frac{1}{s})$ or $1-\beta \sim O(\frac{1}{s})$,

and $s/X^2 \to \infty$ and $X^2 \to \infty$ imply

$$(1-\alpha) \quad \text{or} \quad (1-\beta) \sim \frac{1}{s^r} \quad , \quad 0<r<1$$

This is a vanishingly small region as $s \to \infty$ and will therefore not contribute greatly to the integral.

In Feynman's picture the $\log s$ multiplicity arises from the fact that $E.\,d\sigma/d^3p$ has a plateau which grows as $\log s$ when plotted in rapidity (Fig.1). Consequently the above integral increases as $\log s$ due to an increasing number of pionized particles. In the Yang picture (Fig.2) it arises from the increasing number of fast fragments(x).

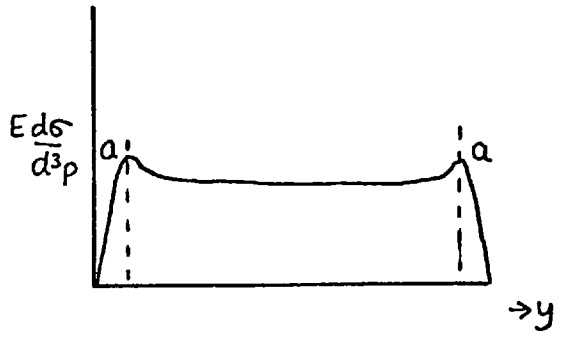

Fig. 1

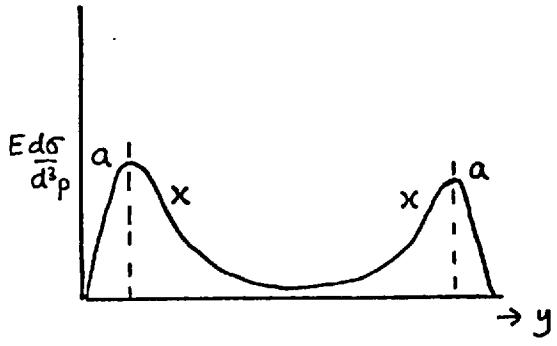

Fig. 2

The regions of phase space where X^2 is small or s/X^2 and $X^2 \to \infty$ are at the very ends of the rapidity plots and contribute to the constant

term. In both pictures the fragmentation regions (a) contribute to the constant term (terms ii and iii in equation 4.2).

The log(s) multiplicity has also been obtained in explicit calculations from multiperipheral models (4,42). This is to be expected from the scaling behaviour of such models (4,5).

In this chapter we extend this work to investigate the width of the distribution with a view to considering the nature of this distribution (23). Poisson or Poisson-like distributions are popular candidates (43). Chew and Pignotti (44) proposed a Poisson, albeit in a very simple model. Wang (45) in many fits to experimental data has shown that a Poisson distribution in charged pairs represents the data adequately. He claims it is necessary to consider charged pairs in order to take care of charge conservation. We recall that a Poisson distribution is expected when the particles are emitted completely independently of how many others are emitted or of what momenta they carry.

4.2 The Multiplicity Distribution

Let us first assume that term i in equation 4.2 is valid throughout phase space. We then get

$$\bar{n} = \frac{1}{\sigma(s)} \int g(\underline{K}^2)\, g_a g_b \frac{d^3p}{E} \qquad 4.3$$

which on changing to Sudakov variables becomes

$$\frac{1}{\sigma(s)} \cdot |S| \cdot \int d\alpha\, d\beta\, d^2K\, g(\underline{K}^2)\, \delta(\alpha\beta s + \underline{K}^2 - 1) \qquad 4.4$$

The limits of the α integration are given by

$$\alpha < 1$$
$$\beta < 1 \quad \Rightarrow \quad \alpha > \frac{(1-\underline{K}^2)}{s} \qquad 4.5$$

giving

$$\bar{n}(s) = \int_{\frac{1-\underline{K}^2}{s}}^{1} \frac{d\alpha}{\alpha}\, g_a g_b \int d^2\underline{K}\, g(\underline{K}^2) \cdot \frac{1}{\sigma(s)}$$

$$= \frac{1}{\sigma(s)}\, g_a g_b \left[\left(\int d^2\underline{K}\, g(\underline{K}^2) \right) \ln s - \int d^2\underline{K}\, g(\underline{K}^2) \ln(1-\underline{K}^2) \right] \qquad 4.6$$

in agreement with Mueller to leading order in log(s).

A more realistic calculation would entail chosing some energy $\overline{M^2}$ such that when one of the sub-energies is less than $\overline{M^2}$, term ii or iii is relevant, and when both sub-energies are greater than $\overline{M^2}$ term i is valid. Of course the result must be independent of $\overline{M^2}$. Region i will contribute a log(s) term and ii and iii constant terms.

Let us now calculate the mean width of the distribution. We have

$$\overline{n(n-1)} = \frac{1}{\sigma(s)} \int \left(\frac{d\sigma}{d^3p_c\, d^3p_d} \right) E_c E_d \cdot \frac{d^3p_c}{E_c} \frac{d^3p_d}{E_d} \qquad 4.7$$

by the same arguments as used for the multiplicity, and where c and d are identical particles. If c and d are distinguishable this becomes $\bar{n}_c \cdot \bar{n}_d$.

If we now assume that all the contribution to $\overline{n(n-1)}$ comes from the region where the three Regge pole expansion of the amplitude is valid (chapter II Fig. 6a) and if we extend the region of validity to the whole of phase space, we get

$$\overline{n(n-1)} = \frac{1}{\sigma(s)} \int \prod_{i=1}^{2} \left[\frac{d^3p_i}{E_i}\, g(\underline{K}_i^2) \right] g_a g_b \qquad 4.8$$

which on conversion to Sudakov variables becomes

$$\overline{n(n-1)} = \frac{2|S|^2}{\sigma(s)} \int \prod_{i=1}^{2} d\alpha_i\, d\beta_i\, d^2\underline{K}_i\, \delta(\alpha_i\beta_i s + \underline{K}_i^2 - 1)\, g(\underline{K}_i^2) \times \qquad 4.9$$

$$g_a g_b .$$

where the limits on the α_1, α_2 integrations are determined from the energy momentum constraints

$$\alpha_1 + \alpha_2 < 1$$
$$\beta_1 + \beta_2 < 1 \qquad 4.10$$
$$\alpha_1 > \alpha_2$$

The factor of 2 in equation 4.9 takes care of the fact that we have assumed a specific ordering $\alpha_1 > \alpha_2$,but both orderings contribute to the inclusive cross-section. The region of integration of the variables is the shaded region of Fig. 3 . Then

$$\overline{n(n-1)} = \frac{g_a g_b}{\sigma(s)} \int d^2\underline{K}_1\, d^2\underline{K}_2\, g(\underline{K}_1^2)\, g(\underline{K}_2^2) \times \qquad 4.11$$

$$\ln^2\left[\frac{s}{1-\underline{K}_2^2}\right] \qquad + \text{constants.}$$

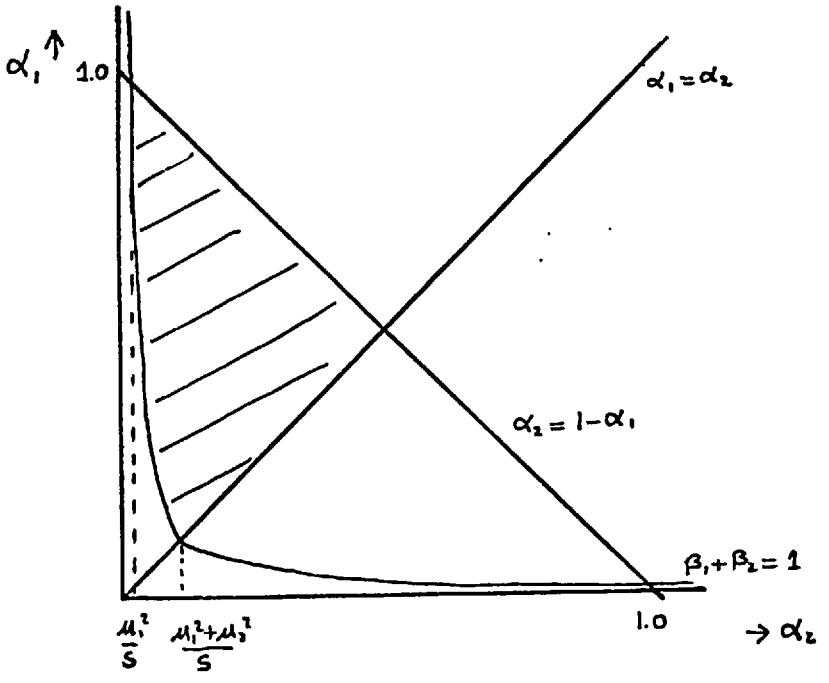

Fig. 3

Now $\sigma(s) = g_a g_b$ so $\overline{n^2} - \bar{n}^2$ (the mean width squared of the distribution) is given by

$$\int d^2\underline{K}_1\, d^2\underline{K}_2\; g(\underline{K}_1^2)\, g(\underline{K}_2^2) \ln\left[\frac{s}{1-\underline{K}_1^2}\right] \cdot \ln\left[\frac{1-\underline{K}_1^2}{1-\underline{K}_2^2}\right] +$$

$$\int d^2\underline{K}\; g(\underline{K}^2) \ln\left(\frac{s}{1-\underline{K}^2}\right) \qquad + \text{constants} \qquad 4.12$$

The log(s) bit of the first term vanishes because the integral

$$\int d^2\underline{K}_1\, d^2\underline{K}_2\; g(\underline{K}_1^2)\, g(\underline{K}_2^2) \ln\left[(1-\underline{K}_1^2)/(1-\underline{K}_2^2)\right]$$

is antisymmetric with respect to exchange of $\underline{K}_1$ and $\underline{K}_2$, whereas physically this should make no difference. This then gives

$$\overline{n^2} - \bar{n}^2 = \bar{n} \qquad + \text{constants} \qquad 4.13$$

Asymptotically, when only the log(s) terms are important, the width squared will be the same as it would be for a Poisson distribution i.e. $\overline{n^2} - \bar{n}^2 = \bar{n}$. This is what we would expect as our particles are emitted independently (expect for some energy-momentum conservation effects) and is essentially similar to the model of Chew and Pignotti (44). This result has been obtained by Webber also (45) in a similar calculation.

4.3 Correlations

The calculation performed in the previous section is somewhat unrealistic, as we would not expect the cross-section to be factorizable everywhere . In general we would expect there to be some correlations between the outcoming particles. That correlations exist is an experimental fact (47). Mueller (48) has defined the correlation functions and shown that if the correlation functions are non-zero only when the relevant sub-energy between the two (or more) particles is small, the integrated correlation functions behave asymptotically as $a \log s + b$. Consequently he was able

to show that we cannot expect a Poisson distribution even at very high energies. In particular the width squared will not equal the mean, though they will be proportional to each other. If we consider our calculation more carefully we are drawn to the same conclusion.

The types of correlations expected may be roughly divided into two classes.

i) Those resulting from conservation laws, such as energy momentum or charge conservation, or

ii) Those resulting from dynamical effects. The most obvious example here is resonances, which play a very important part in two-body and few-body reactions when the sub-energy between two or more particles is small.

We have taken some account of energy momentum conservation in our calculation, in that we have put the correct limits on the phase space integration. However this is not the whole story as the amplitude itself must be modified near the phase space boundary. This can be seen clearly in the work of Brown (49) and Predazzi and Veneziano (50). They define the second correlation function as

$$C_2(p_1, p_2) = N_2(p_1, p_2) - N_1(p_1)\, N_1(p_2) \qquad 4.14$$

where

$$N_2(p_1, p_2) = \frac{1}{\sigma_{tot}} \frac{d\sigma}{\frac{d^3p_1}{E_1}\frac{d^3p_2}{E_2}} \quad , \quad N_1(p_1) = \frac{1}{\sigma_{tot}} \frac{d\sigma}{\frac{d^3p_1}{E_1}} \qquad 4.15$$

The energy-momentum constraints give

$$-p_1 N_1(p_1) = \int dp_2\, p_2\, C_2(p_1, p_2) \qquad 4.16$$

which is to be compared with

$$(p_a + p_b)\, N_1(p_1) = \int d p_2\, N_1(p_1) N_1(p_2)\, p_2 \qquad 4.17$$

The contribution of the correlation function to the sum rule when p_1 is in the pionization region is negligible compared to that from equation 4.17, since $p_{1_0}/(p_a + p_b)_0 \sim 1/s^r$. The contribution is important however when p_1 is in the fragmentation region. Physically this is what we would expect since energy-momentum conservation will have little effect on the pionized particles, as their momenta are negligible compared with those of the incoming particles.(in the centre of mass frame). When both particles are in the same fragmentation region the effect will not be negligible, for example it must prevent both particles from having $\beta(\alpha) > \frac{1}{2}$ simoultaneously. Pictorially the correlation function due to energy-momentum conservation will contribute in the region described by Fig. 4 . This contributes to the constant term in the expression for the width squared and does not affect the log(s) dependence. This is the conclusion of Webber (46) and Bassetto et al (51).

Fig. 4

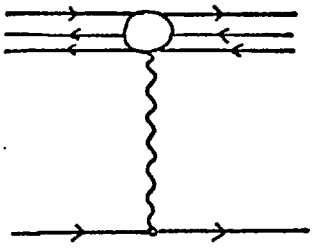

If we have short range dynamical correlations these will contribute in the region described by Fig. 4, but also in the regions described by Figs. 5a→5d . Fig. 5a gives the $\log^2(s)$ term in $\overline{n^2} - \overline{n}^2$, and Figs. 5b and 5c give log(s) terms, and Fig.5d gives a constant term. Since we expect these diagrams and their

discontinuities to be factorizable into products of the separate vertex functions, when we calculate $\overline{n^2} - \overline{n}^2$ we might expect that the contributions due to Fig. 5b cancel with similar terms from $\overline{n}^2$. However no vertex like the central one in Fig. 5c occurs in the single particle cross- section, so we cannot expect this to cancel.

Fig. 5

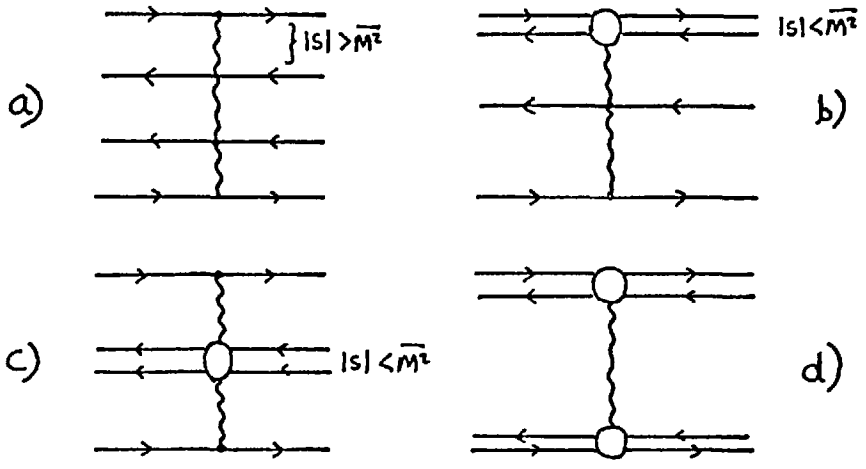

This term for instance could contain contributions from resonance interactions between c and d. So while we would expect that the width squared to vary as log(s), the constant of proportionality will not be the same as in the multiplicity. Thus the distribution cannot be Poisson.

If long range correlations are present, diagrams like Fig. 6 have to be considered. It does not necessarily follow that scaling

Fig. 6

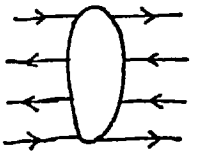

works in this case, and the log(s) predictions for the multiplicity and integrated correlation functions are probably incorrect also. An example of such long range dynamical correlations is the inclusion of cuts in the Mueller diagrams. The conservation laws of momentum and charge induce long range correlations. Charge

conservation has a very definite effect on the log(s) termof the width squared as shown by Brown (48) .

Since we have no model for the 4→4 amplitude (other than the Veneziano model) this approach will not give us quantitative predictions. To do this we are forced to return to specific models for production processes and to work out the correlation functions from these. In Chapter V we take one such model, the multiperipheral model, and calculate the log(s) terms of the multiplicity and width squared.

CHAPTER V

CORRELATION FUNCTIONS IN THE MULTIPERIPHERAL MODEL

5.1 The Model

The multiperipheral model was first proposed by Bertocchi, Fubini and Tonin (52) and Amati, Fubini and Stanghellini (3). Recently the work of Chew, Rogers and Snider (53) has revived interest in the model. The model is a direct generalization of the peripheral model which, for pion exchange processes at low energy, gives quite good results albeit when modified by absorption corrections, (54) or the inclusion of form factors (55). The claim is that the dominant Feynman diagrams for the production of n pions are those where the maximum number of pions is exchanged in the t-channel as in Fig. 1. Here we consider pion-pion scattering. All the solid lines are pions, and each vertex must have an even number of pions to conserve G-parity. 'A' is the pion-pion amplitude with one pion off its mass-shell and 'B' has two pions continued off mass-shell.

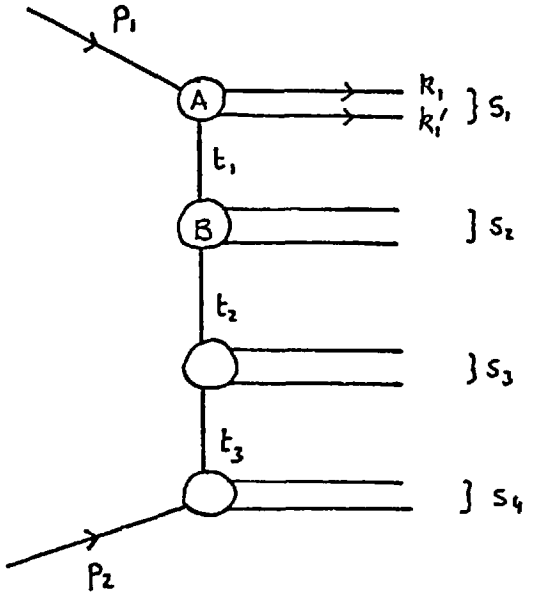

Fig. 1

This model is a much simplified model but incorporates many

of the features of the experimental data, for instance the fact that at high energies, most particles produced are pions. Originally it was assumed that all produced particles are pions, although the model can be modified to include production of Kaons for instance. Also in the original ABFST model the amplitudes A and B were represented by low energy elastic amplitudes to comply with the fact that the average sub-energies of the pions when ordered in their longitudinal momenta is small $\sim 1\,GeV^2$.

In this approximation, the matrix element for Fig. 1 is written as (3)

$$T(p_1 p_2, k_1 k_1') = T^R(s_1,\theta_1,t_1)\cdot\frac{1}{t_1-m_\pi^2}\cdot T^R(s_2,\theta_2,t_1,t_2)\times$$

$$\frac{1}{t_2-m_\pi^2}\cdot T^R(s_3,\theta_3,t_2,t_3)\cdot\frac{1}{t_3-m_\pi^2}\cdot T^R(s_4,\theta_4,t_3) \qquad 5.1$$

where $T^R(s_1,\theta_1,t_1)$ is the elastic $\pi-\pi$ scattering amplitude for sub-energy s_1, scattering angle θ_1, and one of the pions taken off mass shell to $m^2=t_1$. As a first approximation this latter dependence is neglected, i.e.

$$T_1^R(s_1,\theta_1,t_1) \rightarrow T^R(s_1,\theta_1)$$

and $$T^R(s_2,\theta_2,t_1,t_2) \rightarrow T^R(s_2,\theta_2)$$

As mentioned previously the average sub-energy is expected to be small and, to a first approximation, this amplitude is not Reggeized.

The cross-section for production of 2n pions is then

$$\sigma_n(s) = \frac{1}{2q\sqrt{s}\,(8\pi^4)^n}\cdot\iint\frac{d^4q_1\,d^4q_2\cdots d^4q_n\,ds_0\,ds_1\cdots ds_n}{(q_1^2-m_\pi^2)^2(q_2^2-m_\pi^2)^2\cdots\cdots(q_n^2-m_\pi^2)^2}\times$$

$$\delta(k_0^2-s_0)\,2|\underline{k}_0|\sqrt{s_0}\,\sigma^R(s_0)\cdots\delta(k_n^2-s_n)\,2|\underline{k}_n|\sqrt{s_n}\,\sigma^R(s_n) \qquad 5.2$$

with the kinematics defined as in Fig. 2.

$\sigma^R(s)$ is the elastic cross-section at centre of mass energy squared s, q is the modulus of the centre of mass 3-momentum of the colliding pions. $A_n(s)$ is then defined as

$$A_n(s) = 2q\sqrt{s}\,\sigma_n(s) \qquad 5.3.$$

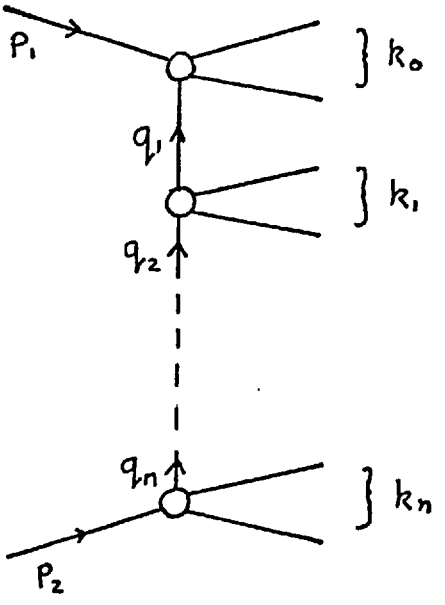

Fig. 2

From the form of $A_n(s)$ it can easily be seen that this satisfies a recursion relation

$$A_n(p,p') = \int ds_0 \frac{A^R(s_0)}{8\pi^4} \int d^4p'' \frac{A_{n-1}(p,p'')\,\delta[(p'-p'')^2-s_0]}{(p''^2-m_\pi^2)^2} \qquad 5.4.$$

Schematically this is shown in Fig. 3.

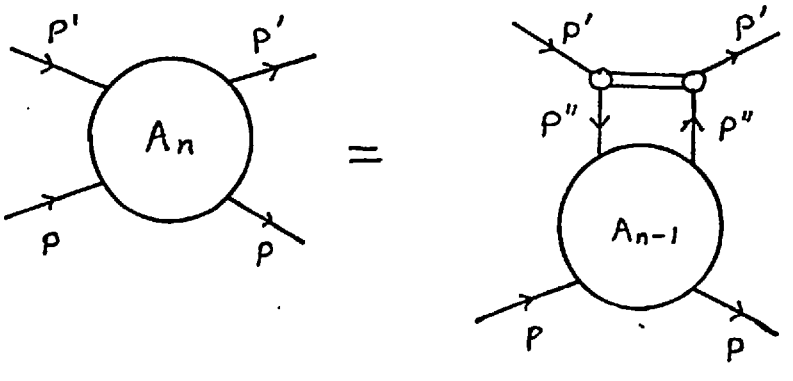

Fig. 3

If we define $A(s,u) = \sum_n A_n(s,u)$

it is clear that $A(s,u)$ satisfies an integral equation

$$A(s,u) = A^R(s,u) + \int ds_0 \frac{A^R(s_0)}{8\pi^4} \iint \frac{ds'du'}{(u'+m_\pi^2)^2} \cdot K(s,u,s',u',s_0)$$

5.5

where u is minus the mass squared of the off mass shell pion $u = -p'^2$. Diagramatically we write this as

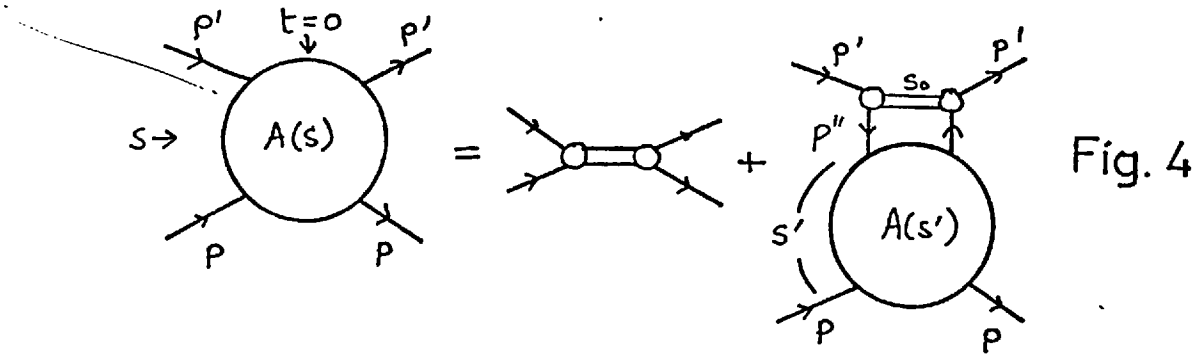

Fig. 4

This is the ABFST integral equation. $A(s,u)$ is identified through unitarity (the optical theorem) as being the imaginary part of the forward amplitude with one pion off its mass-shell. Thus the solution to equation 5.5 is the solution to the unitarity equation in a world where particle production takes place only through multiperipheral graphs.

$K(s,u,s',u',s_0)$ is the Jacobian of transformation from d^4p'' to $ds'du'ds_0$ and is given by

$$\int d^4p'' \, \delta[(p''-p')^2 - s_0] \, \delta[(p''+p)^2 - s'] \, \delta(p''^2+u') \qquad 5.6$$

This equation has been derived for $t \neq 0$ by Bertocchi et al (51). In both this paper and that of AFS (3) one of the most important properties of this solution, namely its Regge behaviour, is derived,

i.e. $$A(s,t,u) \underset{s\to\infty}{\sim} s^{\alpha(t)} \beta(t,u) \qquad 5.7$$

Approximate, but analytic solutions for the Regge poles generated by the ABFST equation have been derived by Goldberger et al (56) and Dash (57). They first take an O(3,1) expansion for t=0, or an O(2,1) expansion for t≠0. Then using various approximations which result in the kernel of the transformed integral equation becoming an infinite sum of seperable terms, they are able to obtain two solutions which correspond to an upper bound solution and a lower bound solution on the trajectories. The trace approximation is also obtained and lies between the two bounds. We will use these approximate solutions in our discussion of the correlation functions.

The solutions are obtained in the form

$$A_L = N_L / D_L + A_{0L} \qquad 5.8$$

A_L is the t-channel partial wave amplitude. D_L is the Fredholm determinant of the integral equation for A_L obtained by the O(2,1) or O(3,1) expansion from the ABFST integral equation. The positions of the Regge poles are determined by the zeros of D_L. A_{0L} is the elastic term.

The behaviour of the integrated correlation functions has been investigated by Mueller (48) within the framework of the AFS model. He found that they are expected to behave as $a \log s + b$ for large s. We hope to be able to predict numerically the asymptotic form of the correlation functions i.e. $a \log s$, by using a specific input kernel. If we are to have any faith in our predictions we must first obtain agreement with the output Pomeron pole, the multiplicity and the width of the distribution.

5.2 The Integrated Correlation Functions

Defining σ_n as the cross-section for producing n particles,

the total cross-section is $\sum_{n=2}^{\infty} \sigma_n$

$\bar{n}$, the average number of produced particles is

$$\bar{n} = \sum_n n\sigma_n \,/\sigma_{tot}$$

and $$\overline{n^2} = \sum_n n^2\sigma_n \,/\,\sigma_{tot} \qquad 5.9$$

Following Mueller (47) the integrated correlation functions may be defined as

$$\begin{aligned} f_1(s) &= \bar{n} \ , \\ f_2(s) &= \overline{n^2} - \bar{n}^2 - \bar{n} \\ f_3(s) &= \overline{n^3} - 3\bar{n}.\overline{n^2} + 2\bar{n}^3 + 2\bar{n} - 3(\overline{n^2} - \bar{n}^2) \end{aligned} \qquad 5.10$$

These formulae result from the definition of correlation functions in terms of inclusive cross-sections

$$\text{e.g.} \quad E_1E_2 \frac{d\sigma}{d^3p_1 d^3p_2} = E_1\frac{d\sigma}{d^3p_1}.E_2\frac{d\sigma}{d^3p_2} + E_1E_2\frac{d\psi}{d^3p_1 d^3p_2} \qquad 5.11$$

where the last term is the correlation function and

$$\int \left[\frac{d\psi}{d^3p_1 d^3p_2}.E_1E_2 \right] \frac{d^3p_1}{E_1}\frac{d^3p_2}{E_2} = f_2(s) \qquad 5.12$$

$\sigma_{tot}(s)$ may be found from the solutions of Dash and Goldberger by the inverse transform

$$Im\left(A(s,t=0)\right) \sim s\,\sigma_{tot}(s) = \int_C \rho_l(z_t)\, dl \left[\frac{N_l}{D_l} + A_{0_l}\right](2l+1) \qquad 5.13$$

where z_t is the t-channel scattering angle. The contour C encloses the Regge poles and includes the background integral.

The usual choice for the input of the ABFST model is the elastic π-π cross-section, which at low energies is represented by the most prominent resonances. Goldberger and Dash chose to represent this contribution by an 'average' zero-width resonance at mass m_0 and with a coupling to two pions of g. This coupling is a measure of the elastic cross-section integrated over the resonance

region. The dynamic off-mass shell dependence is neglected, although the formalism produces kinematic off-shell effects. The D_L function then appears as $1-g^2C_L$ when daughter trajectories are ignored, and the N_L function is proportional to g^4 . Formally we may expand the solution to $\sigma_{tot}(s)$ (eqtn. 5.13) to give us

$$\sigma_{tot}(s) \xrightarrow[s\to\infty]{} \frac{1}{s}\sum_{n=0}^{\infty}\int_C P_L(2L+1)\,N_L\,[g^2C_L]^n\,dL \;+\sigma_2(s) \qquad 5.14$$

The n'th term is proportional to $g^{2(n+2)}$ and we may identify this with the cross-section for $\pi\pi \to (n+2)$ resonances or $2(n+2)$ pions. $\sigma_2(s)$ is the cross-section for producing 2 pions or 1 resonance and is proportional to g^2 . Operating on $\sigma_{tot}(s)$ with $g^2\frac{\partial}{\partial g^2}$ we get

$$\frac{1}{s}\left[\sum_{n=0}^{\infty}\int_C P_L\,dL\,(2L+1)\left[2N_L[g^2C_L]^n + n\,N_L[g^2C_L]^n\right] + \sigma_2\right.$$

$$= \frac{1}{s}\sum_{n=0}^{\infty}\int_C P_L\,dL\,(2L+1)\,N_L(g^2C_L)^n(n+2) + \sigma_2 \qquad 5.15$$

$$= \bar{n}\,\sigma_{tot}(s)$$

and $$\left(g^2\frac{\partial}{\partial g^2}\right)^2\sigma_{tot}(s) = \sigma_2 +$$

$$\frac{1}{s}\sum_{n=0}^{\infty}\int_C P_L\,dL\,(2L+1)\,(n+2)^2\,N_L(g^2C_L)^n = \overline{n^2}\,\sigma_{tot}(s) \qquad 5.16$$

and $$\left(g^2\frac{\partial}{\partial g^2}\right)^3\sigma_{tot}(s) = \overline{n^3}\,\sigma_{tot}(s) \qquad 5.17$$

Now let us assume that $\sigma_{tot}(s)$ is given by Regge poles i.e. $\sigma_{tot}(s) = s^{\alpha_0-1}\beta(0)$ + lower poles and cuts. α_0 is the leading trajectory and $\beta(0)$ its residue, both measured at t=0. It is generally assumed that multiperipheral models do not generate a Pomeron at exactly $\alpha_0 = 1$, and so the cut contributions die away as an inverse fractional power of s. If α_0 is exactly 1 the cut contributions die away as $1/\log^n s$ (unless there are an infinite number of cuts). Consequently at high energy we will keep

only the leading pole term and assume the cuts to be unimportant.

Then $$\sigma_{tot} = s^{\alpha_0 - 1}\,\beta(0) \qquad 5.18$$

$$g^2\frac{\partial}{\partial g^2}\left[s^{\alpha_0-1}\beta(0)\right] = s^{\alpha_0-1} g^2\frac{\partial\beta}{\partial g^2} + \log s\; s^{\alpha_0-1}\beta\; g^2\frac{\partial\alpha_0}{\partial g^2}$$

$$= \bar{n}\; s^{\alpha_0-1}\beta(0) \qquad 5.19$$

giving $$\bar{n} = g^2\frac{\partial\alpha}{\partial g^2}\log s + g^2\frac{\partial\beta}{\partial g^2}/\beta \qquad 5.20$$

Similarly

$$\overline{n^2} - \bar{n}^2 = \left[g^4\frac{\partial^2\alpha}{\partial g^4} + g^2\frac{\partial\alpha}{\partial g^2}\right]\log s +$$

$$+ g^2\frac{\partial\beta}{\partial g^2}/\beta + g^4\frac{\partial^2\beta}{\partial g^4}/\beta - \left[g^2\frac{\partial\beta}{\partial g^2}/\beta\right]^2 \qquad 5.21$$

which gives $$f_2 = g^4\frac{\partial^2\alpha}{\partial g^4}\log s + g^4\frac{\partial^2\beta}{\partial g^2}/\beta - \left[g^2\frac{\partial\beta}{\partial g^2}/\beta\right]^2 \qquad 5.22$$

and

$$\overline{n^3} = \log^3 s\left(g^2\frac{\partial\alpha}{\partial g^2}\right)^3 + \log^2 s\left[3g^4\frac{\partial^2\alpha}{\partial g^4}\,g^2\frac{\partial\alpha}{\partial g^2} + 3\left(g^2\frac{\partial\alpha}{\partial g^2}\right)^2\right.$$

$$\left. + 3\left(g^2\frac{\partial\alpha}{\partial g^2}\right)^2 g^2\frac{\partial\beta}{\partial g^2}/\beta\right] + \log s\left[g^6\frac{\partial^3\alpha}{\partial g^6} + 3g^4\frac{\partial^2\alpha}{\partial g^4} +\right.$$

$$\left. 6g^2\frac{\partial\alpha}{\partial g^2}\cdot g^2\frac{\partial\beta}{\partial g^2}/\beta + 3g^4\frac{\partial^2\beta}{\partial g^4}/\beta\cdot g^2\frac{\partial\alpha}{\partial g^2} + g^2\frac{\partial\alpha}{\partial g^2}\right] +$$

$$\left[g^6\frac{\partial^3\beta}{\partial g^6} + 3g^4\frac{\partial^2\beta}{\partial g^4} + g^2\frac{\partial\beta}{\partial g^2}\right]/\beta \qquad 5.23$$

This gives

$$f_3 = \log s\left(g^6\frac{\partial^2\alpha}{\partial g^6}\right) + g^6\frac{\partial^3\beta}{\partial g^6}/\beta$$

$$+ 2\left(g^2\frac{\partial\beta}{\partial g^2}/\beta\right)^3 - 3g^2\frac{\partial\beta}{\partial g^2}/\beta\cdot g^4\frac{\partial^2\beta}{\partial g^4}/\beta \qquad 5.24$$

Generalizing to the n'th correlation function the coefficient of the $\log s$ term is $g^{2n}\,\partial^n\alpha/\partial g^{2n}$ which is the result of Mueller (48).

We may now use the solutions of Dash for the leading Regge

pole generated by the ABFST model to evaluate this quantity. In fact to calculate the coefficient of the logarithm in the integrated correlation function we need only consider the D_ι function. If we want to calculate the constant terms we must also evaluate the N_ι function.

The Regge pole position is given by the zero of D_ι i.e. α is the solution to

$$1 - g^2 C_\alpha = 0 \qquad 5.25$$

Differentiating with respect to g^2 we get

$$C_\alpha + g^2 \frac{\partial C_\alpha}{\partial \alpha} \cdot \frac{\partial \alpha}{\partial g^2} = 0$$

or
$$g^2 \frac{\partial \alpha}{\partial g^2} = - C_\alpha \Big/ \partial C_\alpha / \partial \alpha \qquad 5.26$$

Differentiating again we have

$$2 \frac{\partial C_\alpha}{\partial \alpha} \cdot \frac{\partial \alpha}{\partial g^2} + g^2 \frac{\partial^2 C_\alpha}{\partial \alpha^2} \left(\frac{\partial \alpha}{\partial g^2}\right)^2 + g^2 \left(\frac{\partial C_\alpha}{\partial \alpha}\right) \frac{\partial^2 \alpha}{\partial g^4} = 0 \qquad 5.27$$

giving
$$g^4 \frac{\partial^2 \alpha}{\partial g^2} = - \frac{\partial^2 C_\alpha}{\partial \alpha^2} \frac{(C_\alpha)^2}{(\partial C_\alpha / \partial \alpha)^3} + \frac{2 C_\alpha}{\partial C_\alpha / \partial \alpha} \qquad 5.28$$

For brevity we write $\frac{\partial C_\alpha}{\partial \alpha} = C_\alpha'$, $\frac{\partial^2 C_\alpha}{\partial \alpha^2} = C_\alpha''$ etc.

We have then

$$g^6 \frac{\partial^3 \alpha}{\partial g^6} = - \frac{1}{C'} \left[C_\alpha''' \left(-\frac{C_\alpha}{C_\alpha'}\right)^3 - 6 C_\alpha'' \left(\frac{C_\alpha}{C_\alpha'}\right)^2 + \right.$$
$$\left. + 3 (C_\alpha'')^2 C_\alpha^3 / (C_\alpha')^4 + 6 C_\alpha \right] \qquad 5.29$$

Thus the coefficients of log (s) in the integrated correlation functions are given by the derivatives of C_α with respect to α

We use the approximate analytic solutions for C_α obtained by Dash (57). For ease of calculation of the derivatives of the functions we use the limits obtained when the mass of the pion is set to zero. This changes the actual numbers somewhat, but we do

not expect that the general features of the solutions are changed. We have checked this by calculations with the true pion mass for the function C_α and its first derivative, and also for the solutions when the mass of the pion is set equal to the mass of the resonance (57). This is an extreme case but shows the same features as the calculation with zero pion mass.

The solutions, neglecting dynamical off mass-shell effects, with the pion mass equal to zero are

1) Lower Bound $$C_\alpha = \frac{\Gamma(\alpha)\,\Gamma(\alpha+1)}{\Gamma(2\alpha+2)}$$

2) Trace Approximation $$C_\alpha = \frac{2}{\alpha(\alpha+1)(\alpha+2)}$$

3) Upper Bound $$C_\alpha = \frac{1}{\alpha(\alpha+1)} \qquad 5.30$$

Demanding a Regge pole at $\alpha \simeq 1$ we obtain the results of Table 1 (the numbers in brackets are the results of calculations using the pion mass equal to the resonance mass.).

	g^2	$\bar{n}/\log s$	$D/\log s$	$\bar{n}_\pi/\log s$	$D_\pi/\log s$
1)	6 (60)	.377 (.48)	.059 (.035)	.503	.104
2)	3	.546	.223	.727	.396
3)	2 (6)	.667 (1.20)	.365 (.64)	.888	.650

Table 1

g^2 is the coupling required to give the Regge pole at $\alpha = 1$ and D is the width squared of the distribution. For a Poisson this is equal to $\bar{n}$.

In the multiperipheral model as formulated here, the multiplicity we have calculated is that of the produced resonances. The experimental quantity which we want to predict is the multiplicity of charged pions. If we assume that the resonances are produced with equal probability of finding a +, - or zero charge, then the number of charged pions is the multiplicity of resonances times 4/3, and similarly the width of the charged distribution is 16/9 times that of the width of the resonances (58).

We notice three points from the above table:

1) the couplings needed to generate poles at $\alpha \simeq 1$ are too large. Chew, Rogers and Snider (53) find that the experimental value of g^2 is 0.8.

2) the width squared is smaller than the multiplicity, whereas the Echo Lake data (59) shows that the width squared is substantially greater than the multiplicity. At accelerator energies however, the width squared is smaller than the mean (60, 61). There appears then to be a change in character of the width squared as the energy increases. The energy dependence of the width squared is thus larger than that of the mean, i.e. the coefficient of the logarithm is larger. At Echo Lake energies the coefficient is about twice as big as that of the mean, although a logarithmic fit is not very satisfactory.

3) the experimental multiplicity measured from the Echo Lake experiment is between 0.6 and 0.8 logs (59). Thus our multiplicities are approximately correct. (To within factors of 2)

The Upper Bound solution gives the best numerical results in that the coupling is only about twice too large. The width squared

is too low however. There is a theoretical objection to this solution, in that it does not satisfy energy conservation. It produces too many particles i.e. $G_n \neq 0$ when n is such that $(nm_\pi)^2 > s$ (62). This is not so for the other two solutions.

The results of this calculation are not very encouraging. A modification of this model, which allows some of the sub-energies of outcoming pions to go large, and which yields a more complicated structure for the Pomeron is the Schizophrenic Pomeron model of Chew and Snider (63, 64). We investigate the predictions of this model for the correlation functions in the next section. This model has the advantage that the resonance coupling need not be so big as in the present case, but the high energy part introduced into the kernel helps boost the trajectory toward 1.

5.3 The Schizophrenic Pomeron

In the model of Chew and Snider (63,64) the production amplitude contains terms where one or more of the sub-energies may become large. Consequently this model contains some Regge exchange in the t-channel (Fig. 5a) and the kernel of the integral equation now has contributions from terms like Fig. 5b. This graph has the structure of the so-called AFS cut (3), but this does not imply that the output 2→2 amplitude has the AFS cut, which from phenomenology is known to have the wrong sign (65). The effect of the inclusion of this term on the D-function in the solution to the equation is to replace $1 - g^2 C_\alpha$ by $1 - g^2 C_\alpha - g_p^4 F_\alpha$ (57, 63, 66) where F_α is the contribution of the box diagram Fig. 5b and g_p is a measure of the coupling strength of two pions to the Reggeon. In the Chew-Snider model this Reggeon is taken to be the Pomeron. An approximate solution to the function F_α has been found

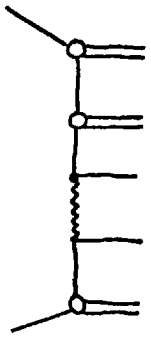

Fig. 5a

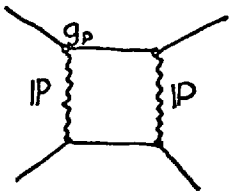

Fig. 5b

by Dash (57) and is given by.

$$F_\alpha(t=0) = I_\alpha^{(1)} I_\alpha^{(2)} \qquad \text{where}$$

$$I_\alpha^{(1)} = \frac{\pi \bar{\beta}^2}{2\alpha' s_0} \left(\frac{s_R}{s_0}\right)^{2\alpha_0 - 1 - \alpha} \left[e^{\frac{k}{\alpha'}[\alpha - 2\alpha_0 + 1]} E_1\left[\frac{k}{\alpha'}[\alpha - 2\alpha_0 + 1]\right]\right]$$

and

$$I_\alpha^{(2)} = \frac{\pi}{4(2\pi)^6} \cdot \Gamma(\alpha+1) \cdot \left(\frac{m_\pi^2}{s_0}\right)^\alpha \cdot \Psi\left(\alpha+2, \alpha+1; \frac{m_\pi^2}{\Delta^2}\right) \qquad 5.31$$

where s_R is the energy below which Regge behaviour is invalid,

s_0 sets the scale of the energy

$\alpha_0 + \alpha' t$ is the input Pomeron trajectory

$\bar{\beta} e^{\gamma t}$ is the Pomeron-pion-pion residue

$k = \gamma + \alpha' \ln(s/s_0)$

Ψ is the confluent hypergeometric function of the second kind and Δ^2 is an effective cut-off on the t-integrations $\sim 1 GeV^2$

Inclusion of this term allows some of the sub-energies to get large. At fixed energy this should have the effect of reducing the mean multiplicity slightly, because there will then be less energy available for producing particles. The effect on the higher correlation functions is discussed below.

The correlations are calculated as before, but now the operator

$g^2 \partial/\partial g^2$ becomes $g^2 \partial/\partial g^2 + g_p^4 \partial/\partial g_p^4$. We have

$$\sigma_{tot} = \frac{1}{s} \sum_{n=0}^{\infty} \int_c P_L \, dL \, (2L+1) \, N_L \left[g^2 C_L + g_p^4 F_L \right]^n + \sigma_2 \qquad 5.32$$

then

$$\bar{n} \, \sigma_{tot} = \left(g^2 \frac{\partial}{\partial g^2} + g_p^4 \frac{\partial}{\partial g_p^4} \right) \sigma_{tot}$$

$$\overline{n^2} \, \sigma_{tot} = \left(g^2 \frac{\partial}{\partial g^2} + g_p^4 \frac{\partial}{\partial g_p^4} \right)^2 \sigma_{tot}$$

$$\overline{n^3} \, \sigma_{tot} = \left(g^2 \frac{\partial}{\partial g^2} + g_p^4 \frac{\partial}{\partial g_p^4} \right)^3 \sigma_{tot} \qquad \text{etc.} \qquad 5.33$$

This is true if the N_L function has the functional form $g^4 M_L + g^2 g_p^4 Q_L + g_p^8 R_L$, or $\left(g^2 M_L' + g g_p^2 Q_L' + g_p^4 R_L' \right)^2$ (67). This is expected to be true as the N_L function is the box graph i.e. it is related to the 2→4 cross-section. Chew and Snider (64) in fact argue that the N_L function is approximately that of the resonance solution only, because of the smallness of g_p^4 compared to g^2.

Then we have

$$\bar{n} = \left[g^2 \frac{\partial \alpha}{\partial g^2} + g_p^4 \frac{\partial \alpha}{\partial g_p^4} \right] \log s + \text{const.} \qquad 5.34$$

$$\overline{n^2} - \bar{n}^2 = \left[g^4 \frac{\partial^2 \alpha}{\partial g^4} + 2 g^2 g_p^4 \frac{\partial^2 \alpha}{\partial g^2 \partial g_p^4} + g_p^8 \frac{\partial^2 \alpha}{\partial g_p^4} + g^2 \frac{\partial \alpha}{\partial g^2} + g_p^4 \frac{\partial \alpha}{\partial g_p^4} \right] \log s + \text{const.} \qquad 5.35$$

giving $f_2 = \left[g^4 \frac{\partial^2 \alpha}{\partial g^4} + 2 g^2 g_p^4 \frac{\partial^2 \alpha}{\partial g^2 \partial g_p^4} + g_p^8 \frac{\partial^2 \alpha}{\partial g_p^4} \right] \log s + \text{const.}$

$\equiv G^2 \alpha \log s + \text{const.}$ (defining G^2) 5.36

and $f_3 = \left[g^6 \frac{\partial^3 \alpha}{\partial g^6} + 3 g^4 g_p^4 \frac{\partial^3 \alpha}{\partial g^4 \partial g_p^4} + 3 g^2 g_p^8 \frac{\partial^3 \alpha}{\partial g^2 \partial g_p^8} + g_p^{12} \frac{\partial^3 \alpha}{\partial g_p^{12}} \right] \log s + \text{const.} \equiv G^3 \alpha \log s + \text{const.}$ 5.37

The Regge poles are now solutions to

$$1 = g^2 C_\alpha - g_p^4 F_\alpha \qquad 5.38$$

Differentiating with respect to g_p^4 and g^2 respectively we get

$$F_\alpha + g_p^4 F_\alpha' \frac{\partial \alpha}{\partial g_p^4} + g^2 C_\alpha' \frac{\partial \alpha}{\partial g_p^4} = 0$$

$$C_\alpha + g^2 C_\alpha' \frac{\partial \alpha}{\partial g^2} + g_p^4 F_\alpha' \frac{\partial \alpha}{\partial g^2} = 0 \qquad 5.39$$

giving

$$g^2 \frac{\partial \alpha}{\partial g^2} + g_p^4 \frac{\partial \alpha}{\partial g_p^4} = - \frac{(g^2 C_\alpha + g_p^4 F_\alpha)}{g^2 C_\alpha' + g_p^4 F_\alpha'} \qquad 5.40$$

Similarly

$$G^2\alpha = - \frac{(g^2 C_\alpha'' + g_p^4 F_\alpha'')}{(g^2 C_\alpha' + g_p^4 F_\alpha')^3} \cdot (g^2 C_\alpha + g_p^4 F_\alpha)^2 + 2 \cdot \frac{g^2 C_\alpha + g_p^4 F_\alpha}{g^2 C_\alpha' + g_p^4 F_\alpha'} \qquad 5.41$$

and

$$G^3\alpha = - \frac{1}{g^2 C_\alpha' + g_p^4 F_\alpha'} \cdot \left[(g^2 C_\alpha''' + g_p^4 F_\alpha''') \left(- \frac{g^2 C_\alpha + g_p^4 F_\alpha}{g^2 C_\alpha' + g_p^4 F_\alpha'} \right)^3 - 3 (g^2 C_\alpha''' + g_p^4 F_\alpha''') \left[2 \left(\frac{g^2 C_\alpha + g_p^4 F_\alpha}{g^2 C_\alpha' + g_p^4 F_\alpha'} \right)^2 - \frac{(g^2 C_\alpha'' + g_p^4 F_\alpha'')(g^2 C_\alpha + g_p^4 F_\alpha)^3}{(g^2 C_\alpha' + g_p^4 F_\alpha')^4} \right] + 6 (g^2 C_\alpha + g_p^4 F_\alpha) \right] \qquad 5.42$$

The function F_α has a logarithmic singularity at $\alpha = 2\alpha_0 - 1$ Consequently the predictions of the model are very dependent on the positions of the output and input poles. The partial bootstrap, proposed by Chew and Snider (64) however, greatly constrains the model and we will use their results to fix any free parameters at reasonable values. Their bootstrap scheme equates the input and output Pomeron. This makes $\alpha_p(0) = 1$ a singular point, so we have $\alpha_p(0) < 1$ unless its coupling vanishes. Since α_p is chosen to be near 1 in order to account for the near constancy of total cross-sections we are necessarily very near the singularity of the F-function. The scheme also equates the input γ to the output γ in the residue function.

As a first approximation we will use the same form of the F-functions as Chew and Snider. This means we neglect the $I_\alpha^{(2)}$

function, which because of its slowly varying nature in l, should not be a very serious omission.

$$g_p^4 F_\alpha = g_p^4 \frac{\gamma}{\alpha'} e^{\frac{\gamma}{\alpha'}[\alpha - 2\alpha_0 + 1]} E_1\left[\frac{\gamma}{\alpha'}[\alpha - 2\alpha_0 + 1]\right] \qquad 5.43$$

Now

$$\frac{\partial}{\partial l} e^l E_1(l) = e^l E_1(l) - \frac{1}{l} \qquad 5.44$$

and so

$$g_p^4 \frac{\partial F_\alpha}{\partial \alpha} = g_p^4 \frac{\gamma}{\alpha'}\left[\frac{\gamma}{\alpha'} e^{\frac{\gamma}{\alpha'}[\alpha - 2\alpha_0 + 1]} E_1\left[\frac{\gamma}{\alpha'}[\alpha - 2\alpha_0 + 1]\right] - \frac{1}{\alpha - 2\alpha_0 + 1}\right] \qquad 5.45$$

Thus if the Pomeron intercept α_0 is close to 1, the successive derivatives of F_α with respect to α, at the Pomeron pole are increasingly larger as shown in Table 2. The parameters chosen are $\gamma/\alpha' = 10$, $\alpha_0 = .97$.

F_α	F_α'	F_α''	F_α'''
12.5	-210	9,000	-72,000

Table 2.

The C-function on the other hand is a much more slowly varying function and its successive derivatives do not increase so rapidly. As an example the first three derivatives of our $m_\pi = 0$ approximations are shown below in Table 3.

This illustration shows that, although g_p^4 may be much smaller than g^2, the effect of the F-function in determining the correlation functions is becoming more important as the order of the correlation function increases, due to the very rapidly increasing successive

derivatives of F_α . Thus while the F-function i.e. the inclusion of

	C_α	C_α'	C_α''	C_α'''
1)	1/6	-.443	1.38	-5.8
2)	1/3	-.61	1.67	-5.13
3)	1/2	-.75	1.75	-7.05

Table 3

the high energy tail of the input kernel, may not affect the determination of the multiplicity, it will affect the shape of the distribution as expressed by the higher moments. Physically this might be expected as the effect of including the Pomeron is to cut down the high multiplicity events in favour of low multiplicities. In particular it turns out that the width of the distribution is increased relative to the case with resonance input only.

Let us now consider the Chew-Snider model in more detail. They assume that the resonance part of the kernel will generate a pole at $\alpha \sim 0.7$ and represent the C-function by a linear function of α. This is a very optimistic choice compared to the approximations used above as will be shown later.

The D-function is then given by

$$D_J = J - a - bt - g_p^4 \varrho_p(t,J) \qquad 5.46$$

where $a+bt$ is the resonance generated pole trajectory. The Pomeron residue is represented by $Ce^{\gamma t}$ with C determined by the condition that $\varrho_p(t,J) \xrightarrow[J\to\infty]{} 1/J$. $\varrho_p(t,J)$ is the box

graph or $I_J^{(1)}(t) \cdot I_J^{(2)}(t)$ in our notation. The bootstrap is then made on $\alpha_p(t)$ and γ. The approximation $I_J^{(2)}(t) = 1$ gives at $t = 0$

$$D_J = J - a - g_p^4 \frac{\gamma}{\alpha'} e^{\frac{\gamma}{\alpha'}[J - 2\alpha_p + 1]} E_1\left[\frac{\gamma}{\alpha'}[J - 2\alpha_p + 1]\right] \quad 5.47$$

and the zeros of this function give the Regge pole positions. The resonance generated pole is associated with the P' and is forced to go through the f_0 (1250 MeV). When the high energy tail is added this pole splits into two as shown below. The real part of the D-function actually has 3 zeros as shown in Fig. 5. The highest value of α is associated with the Pomeron. The second zero at .93 is ignored as the imaginary part of the D-function is very large at that point, so the pole, if there is indeed one, will be very far from the real axis. The third zero at $\sim .6$ is identified with the P'. The way in which this scheme works away from $t = 0$ is discussed by Chew and Snider (64) and Frazer and Mehta (68). At the P' position the imaginary part of D_α is very small.

Two of the sets of self-consistent parameters of Ref. 63 are shown in Table 4.

	g_p^4	$\alpha_p(0)$	α_p'	γ_p	a	b	$\alpha_{p'}(0)$
1)	.02	0.969	0.48	6.1	0.7	0.83	.62
2)	.04	0.936	0.60	3.0	0.7	0.83	.55

Table 4

The multiplicity given by these parameters is

1) $\bar{n} = .167 \log s \qquad \bar{n}_\pi = .222 \log s$

2) $\bar{n} = .345 \log s \qquad \bar{n}_\pi = .46 \log s$

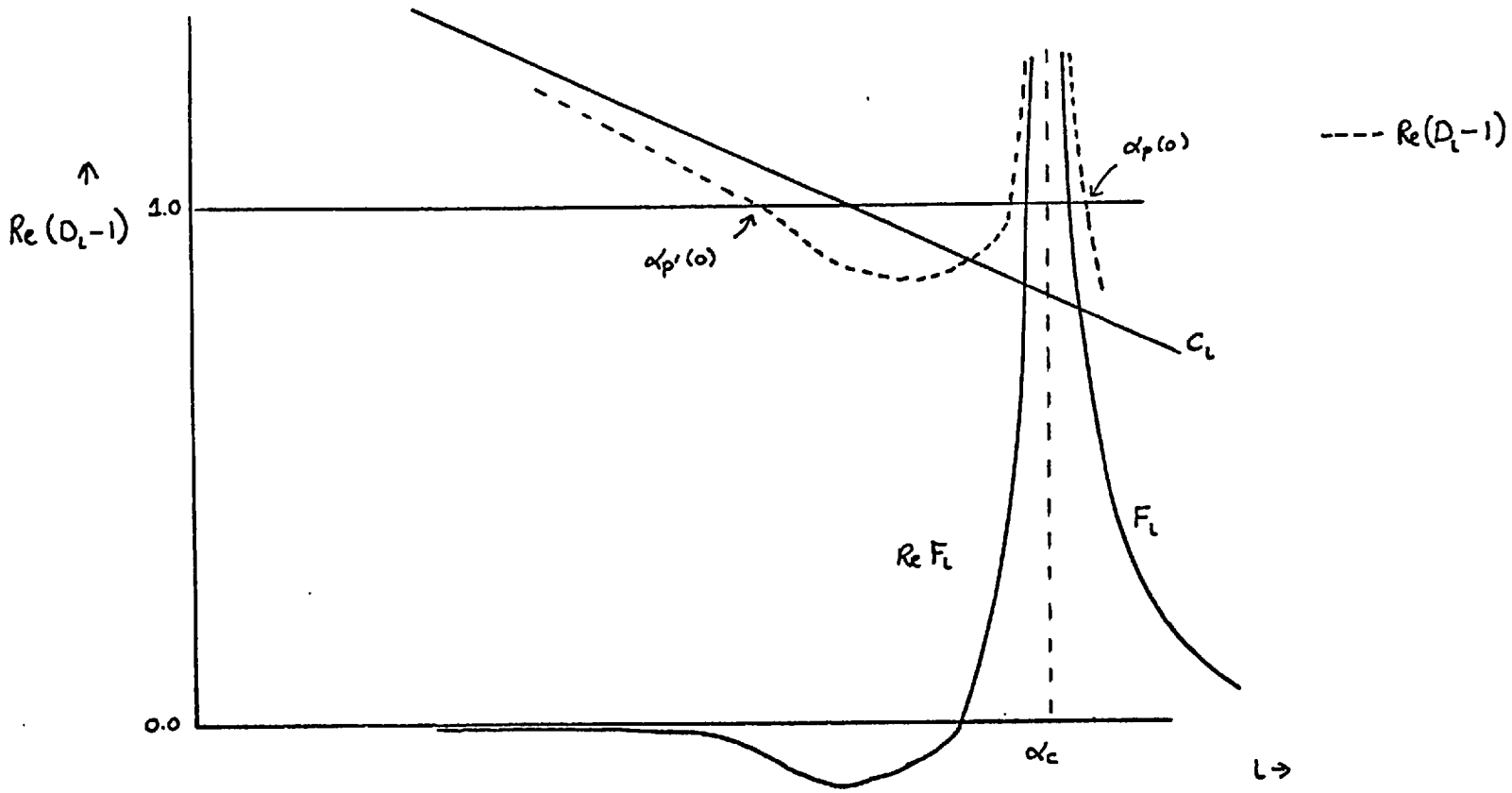

Fig. 5

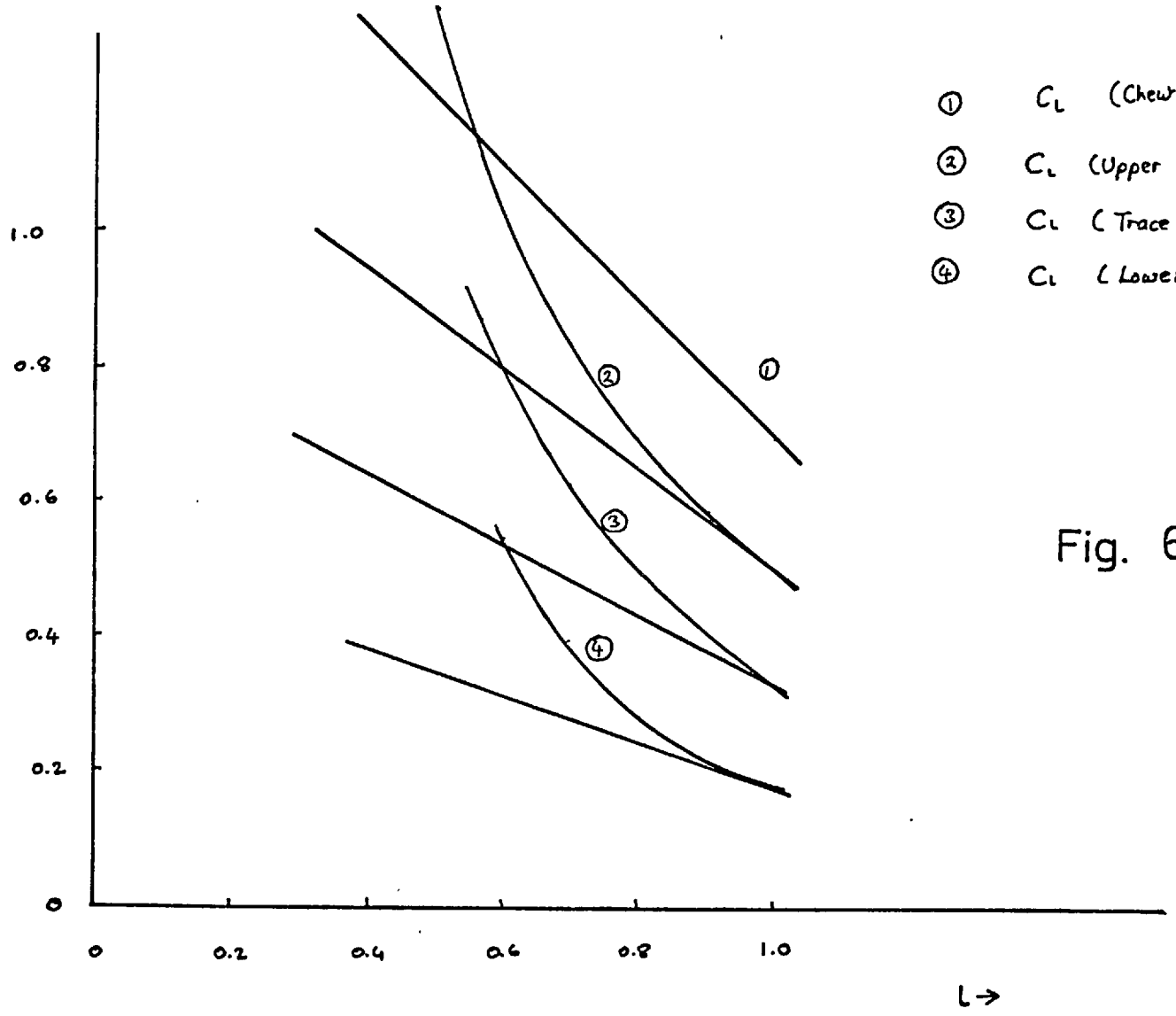
1.0
0.8
0.6
0.4
0.2
0
0
0.2
0.4
0.6
0.8
1.0
L →
① C_L (Chew + Snider)
② C_L (Upper Bound $m_\pi = 0$)
③ C_L (Trace Approx $m_\pi = 0$)
④ C_L (Lower Bound $m_\pi = 0$)

Fig. 6

The charged pion multiplicity generated by the resonance kernel alone would be 4/3 $\log s$. Thus at these values of the parameters the multiplicity is determined largely by the Pomeron. Hence the higher correlation functions will certainly be Pomeron dominated. Notice that the better multiplicity is obtained by moving the Pomeron down to .936. This means that we are moving further away from the singularity of the F-function.

The C-function that Chew uses has no curvature. If we compare the approximate solutions of Dash to that of Chew we find that if we use any of the three approximations discussed earlier, the predictions become worse. This is easily seen in Fig. 6. The approximations are drawn in absolute scale. The C-function of Chew is scaled down to give the same value as the approximate solution at $\alpha \sim .97$ and drawn beside it. i.e. the line drawn by each solution is $(1/G^2).\ C_{c.s_\alpha}$ where G^2 is the number by which the solution must be multiplied to equal the value of Chew's C-function at $\alpha \sim .97$. It can be seen that each of these curves away rapidly from the straight line, thus as t decreases the C-functions increase far more rapidly than the linear approximation of Chew and Snider. This will have the effect of forcing the P' intercept much higher. In fact we found that for reasonable values of the parameters the D-function increased so rapidly away from the cut position that we could not generate the P' pole at all.

We have found, after varying the various parameters, that we are unable in this model to generate

1) a Pomeron pole with intercept
2) a P' pole with intercept
3) an acceptable multiplicity

Consequently we cannot have any faith in predictions for the correlation functions. We assumed that the resonance part of the

kernel could generate a pole at $\alpha \sim .7$, but this requires couplings, g^2, that are too large. ($g^2_{Trace} \sim 1.6$, $g^2_{L.B} \sim 2.54$, $g^2_{U.B} \sim 1.2$) The model as it stands, then, while attractive on a qualitative level, fails when confronted with the experimental data.

Several courses are open to us if we want to modify the model. For instance we could include terms arising from the inclusion of P' in the production amplitude. This would give terms corresponding to the PP' and P'P' cuts in the D-function. The P' could then also be bootstrapped. We have tried this, but again with no success. Dynamic off-mass-shell effects could be taken into account.(this will be discussed further in an extended footnote). However we have been assuming all along that it is the elastic cross-section which is the input kernel of the model. To try to find out how good an assumption this is we carry out the investigation of the integral equation presented in Chapter VI.

FOOTNOTE

As an example of the sort of effects that can be produced by relatively simple off-shell effects we propose the following modification to the vertex function.

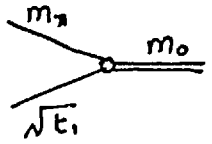

The momentum in the m_0 Centre of Mass frame is given by

$$k^2_{off} = \frac{(m_0^2 - (\sqrt{t_1} - m_\pi)^2)(m_0^2 - (\sqrt{t_1} + m_\pi)^2)}{4m_0^2} \qquad 1$$

We know that the partial wave (ℓ) has a threshold factor k^ℓ, therefore a simple off-mass-shell prescription could be

$$\left(\frac{k_{off}}{k_{on}}\right)^\ell \qquad [\ \ell < \text{some } \ell_{max}\ ] \qquad 2$$

To make the integrals involved in the calculation of the C-function simple, we further approximate this by including in the integral $I^{2,-\lambda-1}_{2\lambda+1}$ which appears in the lower bound solution to $C_\alpha^{(nn)}$ (see Eqtn. 3a in note added in proof to Ref. 57(i)), a term $((y + m_0^2)/m_0^2)^2$ which results in

$$C_\alpha^{(nn)}\Big|_{\substack{\text{modified} \\ \text{L.B.}}} = \frac{g^2}{\lambda+1}\, m_0^{2(\lambda-2)}\, I^{2,1-\lambda}_{2\lambda-1} \qquad 3$$

The $m_\pi = 0$ approximation is

$$C_\alpha^{(00)} = \frac{1}{\alpha+1}\,\frac{\Gamma^2(\alpha)}{\Gamma(2\alpha)} \qquad 4$$

This gives us the results of Table 1 (in the same notation as Chapter V)

g^2	$\bar{n}/\log s$	$D/\log s$	$\bar{n}_\pi/\log s$	$D_\pi/\log s$
2	.4	.06	.53	.107

Thus the coupling required to produce a pole at $\alpha = 1$ is a factor of 3 down on the unmodified lower bound solution. It can be seen however that the multiplicity distribution obtained suffers from the same defects as the unmodified versions. It would appear then that a fairly simple off-mass-shell prescription could fix up the problem of the coupling, but we suspect that a more drastic change is needed to alter the shape of the distribution. There is another objection to this sort of prescription, and that is that it increases the average value of the momentum transfer - as can be seen by studying the integrand

$$\frac{(-t)^{L+1}}{(m_\pi^2-t)^2}\cdot\frac{1}{(m_o^2-t)^{2L+2}} \rightarrow \frac{(-t)^{L+1}}{(m_\pi^2-t)^2}\cdot\frac{1}{(m_o^2-t)^{2L}} \qquad 5$$

This is the sort of off-mass-shell effect that is considered by Avalos and Webber (72).

CHAPTER VI

THE KERNEL OF THE ABFST INTEGRAL EQUATION

6.1 Introduction

In the previous chapter it was supposed that the resonance part of the AFS kernel could generate a Regge pole with $\alpha(0) \sim .7$. With our approximations for the solutions to the equation this required a coupling that was too big. That the resonance portion of the kernel is unable to produce a high lying Regge pole has been known for some time. In particular Tow (42) and Chew, Rogers and Snider (53) have investigated the predictions of the ABFST model with an up-to-date guess for the elastic π-π cross-section. They found in fact that this generated a Pomeron pole with an intercept of $\sim .3$ and a ρ pole with intercept $\sim .2$. Chew, Rogers and Snider (hereafter called CRS) also included a high energy Pomeron component in the elastic cross-section but this did not improve matters much. In both papers the amplitudes were treated as being completely on-shell. Tow however has investigated some off-mass-shell prescriptions and claims that they either have the effect of decreasing the kernel strength, or increasing the average momentum transfer and thus undermining one of the basic principles of multi-peripheralism. CRS point out that another possible source of error is the omission of crossed graphs. Snider and Tow (69) have considered the effect of some of the more important crossed graphs (Fig. 1). They conclude that, while these terms are important in evaluating exclusive cross-sections (in agreement with the conclusions of Jurewicz et al (70)) they have a very small effect on the position of the leading Regge pole. They consider only a small subset of the possible graphs that could be included.

Fig. 1

We note that the structure of the integral equation is unchanged by including many crossed terms i.e. if we define the kernel K by

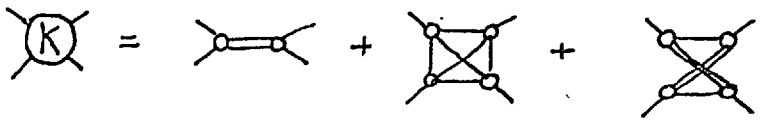

6.1

we can still write

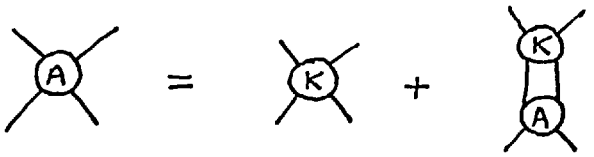

6.2

Various other schemes for boosting the effect of the resonances have been proposed. Wyld (71) has included SU(3) multiplets instead of just pions. Avalos and Webber (72) have described an off-mass-shell technique. Both schemes improve the strength of the kernel but not sufficiently to produce a high lying Pomeron.

Rather than guessing at the form of the kernel we (73) reverse the problem. Given the total cross-section we solve for the irreducible kernel I, defined diagramatically in Fig. 2.

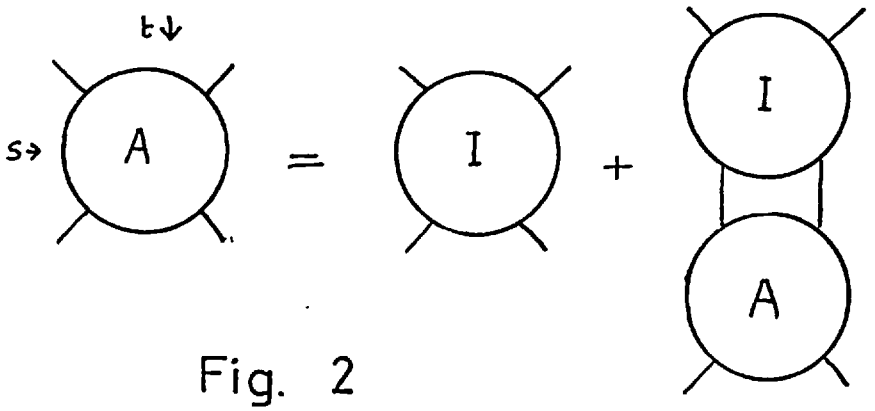

Fig. 2

Since we do not know how to take the amplitudes off-shell we will regard them as objects with all four pions on mass-shell, but impose certain cut-offs on the momentum transfers carried by the pions to simulate mass-shell effects. The hope originally was that if the high energy part of the kernel were unimportant and reduced to zero at some finite energy, we could solve for this kernel and then use it to predict the forward amplitude at any energy.

We consider only the $I_t=0$ component of the kernel as we specifically want to investigate the generation of the Pomeron. Since we want the solution at all energies we do not make any partial wave decompositions.

6.2 The π-π Cross-Sections

We use the same parameterizations as CRS for the elastic and total cross-sections. At low energies we include all the resonances shown in the Table below. For the high energy components $\sigma_{tot}^{\pi\pi}$ is 16 mbs. and $\sigma_{el}^{\pi\pi} \sim 3$ mbs. at around 10-20 GeV^2.

Resonance	Mass (GeV)	Spin	Isospin	Full width (GeV)	Elasticity $\Gamma_{\pi\pi}/\Gamma_{tot.}$
ρ	0.765	1	1	0.14	1.0
ϵ	0.765	0	0	0.45	1.0
f	1.26	2	0	0.14	1.0
g	1.65	3	1	0.14	0.35
f'	1.65	2	0	0.14	0.28

Table: Low Energy Resonance Parameters

With the normalization we have used

$$\sigma_{tot}^{I} = \frac{16\pi}{2k^2} \sum_{L} (B.W)_{L}^{I} (B.W)_{L}^{I*} (2L+1) \qquad 6.3$$

where I refers to the Isospin, L the spin and k is the centre of mass momentum of two-pion system.

$(B.W)_{L}^{I}$ is the Breit Wigner amplitude

$$\frac{M_R \Gamma}{(M_R^2 - s) - i M_R \Gamma} \qquad 6.4$$

where M_R is the mass of the resonance, Γ is the full width, and s is the centre of mass energy squared of the two pion system.

To get the elastic cross-section the width in the numerator is multi-plied by the elasticity X, i.e.

$$\sigma_{el}^{I} = \frac{8\pi}{k^2} \sum_{L} \frac{(M_R \Gamma X)^2}{(M_R^2 - s)^2 + (M_R \Gamma)^2} \qquad 6.5$$

To prevent this blowing up at threshold we include factors which take into account the change in Γ with k. This gives us the correct threshold behaviour (74). Jackson's prescription is to take $\Gamma \to \Gamma (k/k_R)^{2L+1}$ where L is the spin of the resonance and $k_R = \sqrt{M_R^2 - 4m_\pi^2}$. For large k this gives $(B.W)\times(B.W)^* \to 1$ for $L \gg 1$. So we modify this prescription to $\Gamma \Rightarrow \Gamma (k/\omega)^{2L+1}$ which changes the normalization of the resonances slightly, but only by about 4% at the ρ peak where the effect is greatest. For the ϵ resonance however, we retain the k/k_R prescription, as the k/ω method gives a threshold value for the cross-section of ~ 100 mbs. The k/k_R prescription gives the more reasonable 15 mbs. Parameterized in this fashion, our expression for σ_{el} agrees well with that of CRS.

Since we want to determine the solutions for a specific

Regge pole - namely the Pomeron - we diagonalize the equation in terms of t-channel Isospin. To obtain the Pomeron we need $I_t = 0$ (t-channel Isospin component of 0). The contribution of the elastic cross-section to the t-channel $I=0$ state is then $\beta_{oI}\,\sigma_{el}{}^{I}$, and similarly the contribution of the total cross-section is $\beta_{oI}\,\sigma_{tot}{}^{I}$ where $\beta_{II'}$ is the Isospin crossing matrix.

$$\beta_{II'} = \begin{pmatrix} \frac{1}{3} & 1 & \frac{5}{3} \\ \frac{1}{3} & \frac{1}{2} & -\frac{5}{6} \\ \frac{1}{3} & -\frac{1}{2} & \frac{1}{6} \end{pmatrix} \qquad 6.6$$

When considering the $I_t = 0$ total cross-section we added a constant high energy tail of $16\,mbs$ which we continued down through the resonance region, parameterized by $16\sqrt{(s-4m_\pi^2)/s}$. It may be argued that we have neglected other contributions to the high energy tail, such as the P'. However we did not cut off the resonances, so their high energy tails may be regarded as building up the P' contribution, by appealing to the two component duality hypotheses of Freund and Harari (14, 15). The effective P' contribution built up in this way is very small however. Our conclusions will be independent of such details.

To the $I_t = 0$ elastic cross-section we add a high energy tail of $3 / \log(s/s_o)\,mbs$.. This is parameterized as $3\sqrt{(s-4m_\pi^2)/s}$ until $\log(s/s_o)$ is 1, then it is replaced by $\sqrt{(s-4m_\pi^2)/s}\,.\,3/\log(s/s_o)$ The scale factor s_0 is chosen to be 1. This procedure adds an almost constant contribution to the low energy component of $\sigma_{el}{}^{I_t=0}$ This may be identified with the $I_s = 2$ component of $9-12\ mbs$.

which CRS include as a non-resonant background.

6.3 Predictions of the ABFST Model

In this section we present the solutions of the ABFST equation using as input the kernel that corresponds to the elastic cross-section. The positions of the Regge poles generated in this manner have been obtained by CRS and Tow. We solve for $Im A(s, t=0)$ numerically.

Returning to equations (5.5) and (5.6) of Chapter V and following AFS (3) we define

$$S = s + u - m_\pi^2 ,$$
$$S' = s' + u' - m_\pi^2 ,$$
$$S_0 = s_0 + u + u' \qquad 6.7$$

$K(s,u,s',u',s_0)$ becomes $\frac{\pi}{2\sqrt{S^2+4m_\pi^2 u}} \cdot \Theta(\sqrt{s}-\sqrt{s'}-\sqrt{s_0}) \times$

$$\Theta(uS'^2 + u'S^2 - m_\pi^2 S_0^2 - SS'S_0 + 4m_\pi^2 uu') \qquad 6.8$$

where Θ is the step-function.

The second term on the right hand side of equation 5.5 becomes

$$\int_{4m_\pi^2}^{s_{0max}} ds_0 \, \frac{A^R(s_0)}{8\pi^4} \cdot \frac{\pi}{2\sqrt{S^2+4m_\pi^2 u}} \int_{4m_\pi^2}^{s'_{max}} ds' \int_{u_{min}}^{u_{max}} du' \, \frac{A(s',u')}{(u'+m_\pi^2)^2} \qquad 6.9$$

where

$$s'_{max} = (\sqrt{s}-\sqrt{s_0})^2 ,$$
$$s_{0\,max} = (\sqrt{s}-2m_\pi)^2 ,$$
$$u_{max} = a + b ,$$
$$u_{min} = a - b ,$$

where

$$a = \frac{s - s' - s_0 - 2m_\pi^2}{2} ,$$

$$b = \left(\left(\frac{s-s'-s_0-2m_\pi^2}{4}\right)^2 - \frac{1}{s}\left(m_\pi^2(s'-s_0)^2 + ss's_0 - m_\pi^2 s(s'+s_0)\right)\right)^{\frac{1}{2}} \qquad 6.10$$

If we now assume that $A(s,u)$ has no u dependence, (i.e. $u = -m_\pi^2$) the u' integration may be done explicitly, leaving us with a two-dimensional integral equation. The order of the s_0 and s' integration is interchangeable, and the S_0 integration was performed numerically using Gaussian quadrature. This leaves us with an integral equation of the form

$$A(s) = I(s) + \int_{4m_\pi^2}^{(\sqrt{s}-2m_\pi)^2} F(s,s')\,A(s')\,ds' \qquad 6.11$$

which is Volterra. Thus $F(s,s')$ need only be known for $s' \leq s$. Consequently when the integral is reduced to a Gaussian integration so that the integral becomes a matrix equation, the matrix is lower triangular. The inversion of this equation is discussed in the Appendix.

In an attempt to discover something about the dependence of $A(s,u)$ on u we examine the effect of cutting off the u' integration at arbitrary values. This method of putting in 'off-mass-shell' effects has the advantage of still leaving the u' integration tractable. CRS were obliged to put such a cut-off on the u' integration over the high energy tail in order to make their integrals converge for large s.

Fig. 3 shows the results of our calculations with input kernel $2k\sqrt{s}\,\sigma_{el}^{I_t=0}$.

Curve a is $2k\sqrt{s}\,\sigma_{el}^{I_t=0}$.

Curve b is the result of the calculation of CRS with a cut-off on the u' integration at $1\,GeV^2$ for $s_0 > 3\,GeV^2$. The leading output trajectory has an intercept of ~ 0.4 . The intercept with no high energy tail to the kernel was ~ 0.2.

Curve c corresponds to a u' cut-off at 1 GeV^2 for all s_0 values.

Curves d and e correspond to multiplying the resonance part of the elastic cross-section by 3.0 and 4.2 respectively while keeping the

Fig. 3

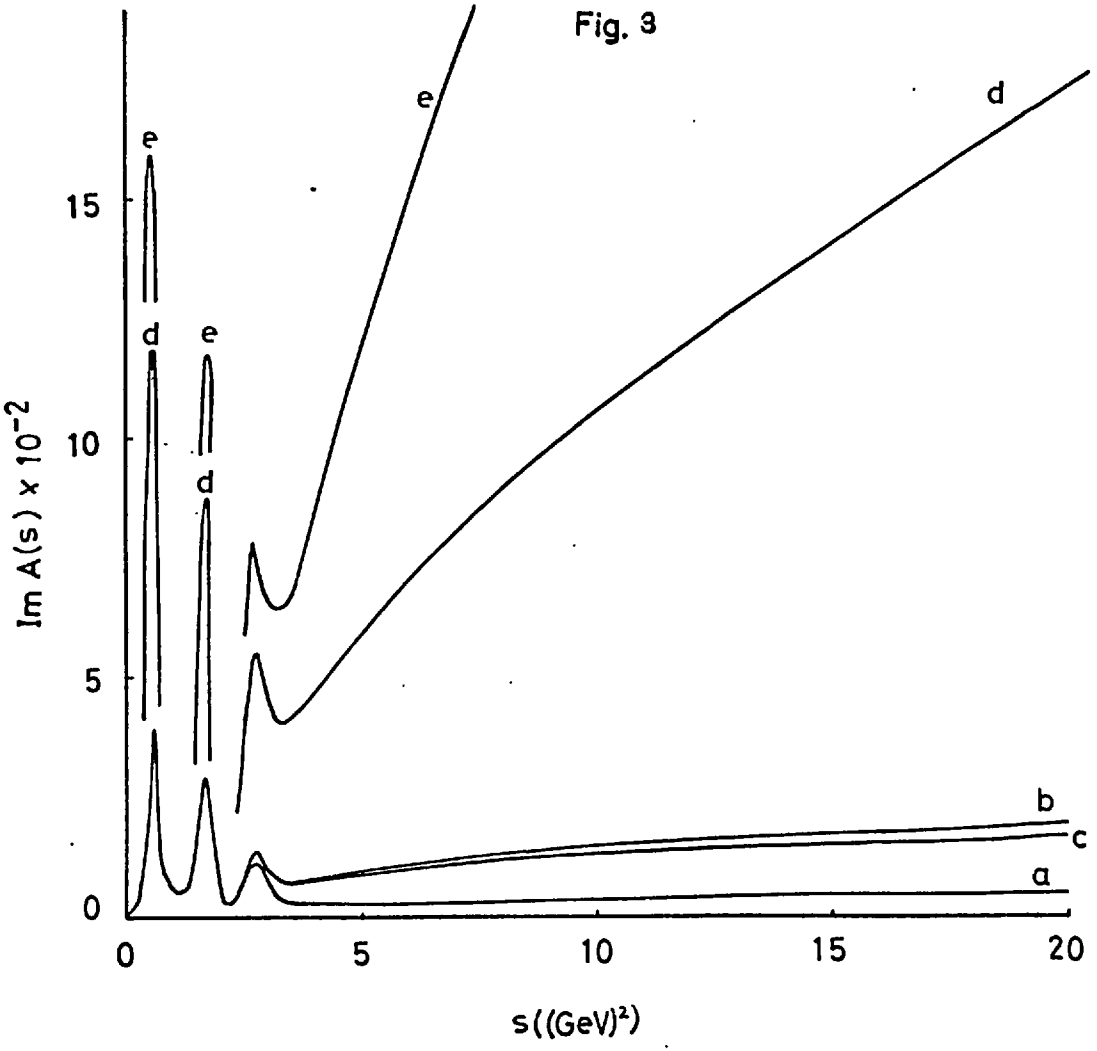

cut-off on the u' integration for $s_0 > 3\text{GeV}^2$. The leading trajectories are now at $\alpha(0) \sim 0.7$ and $\alpha(0) \sim 1.0$ respectively. The total cross-section corresponding to the $\alpha(0) \sim 1.0$ solution is ~ 80 mbs. agreeing reasonably well with the estimate of Abarbanel et al (75).

While it is true that multiplying the input kernel by some number will give a leading trajectory where desired, the shape and normalization of the imaginary part of the amplitude that results is completely wrong (c.f. Fig. 4 curve a). Thus the changes that are required in the kernel are more subtle than mere multiplication by factors.

6.4 The Kernel

Now regarding $A(s,u)$ as known we solve for the irreducible kernel (irreducible with respect to two pions in the t-channel). Again no explicit u-dependence is included, but we cut off the integration at various values to exhibit the importance of off-mass-shell effects. Fig. 4 shows the results we obtained.

Curve a is the input $A(s,m_\pi^2) = 2k\sqrt{s}\ \sigma_{tot}^{I_t=0}$
If we put no u' cut-off on the integration, the solution for the kernel is given by curve d. Curve e is $2k\sqrt{s}\,\sigma_{el}^{I_t=0}$ included here for comparison. Curve b is obtained when a u' cut-off is included for all s_0, and curve c when the u' cut-off is included only for $s_0 > 3\text{GeV}^2$. The latter is an attempt to derive the kernel that CRS should have used.

These curves show very explicitly that the shape of the kernel required is very different from that corresponding to the elastic cross-section. In particular at the high mass resonances the kernel looks much more as if it were generated by σ_{tot}. . The high energy tail is much bigger than that suggested by CRS and is diverging away from their guess at $s = 20\ \text{GeV}^2$. Another point to notice is that the cut-off

Fig. 4

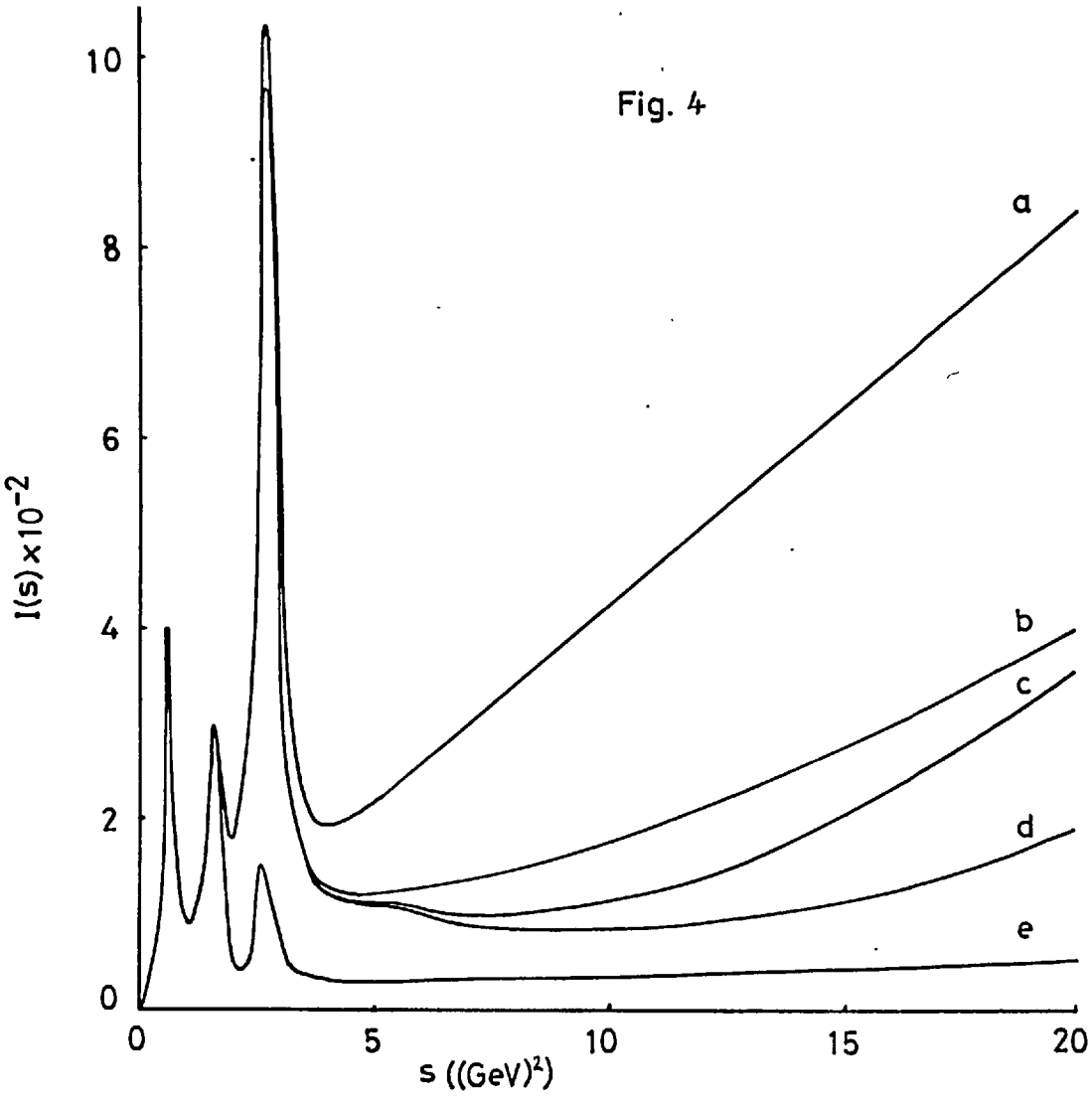

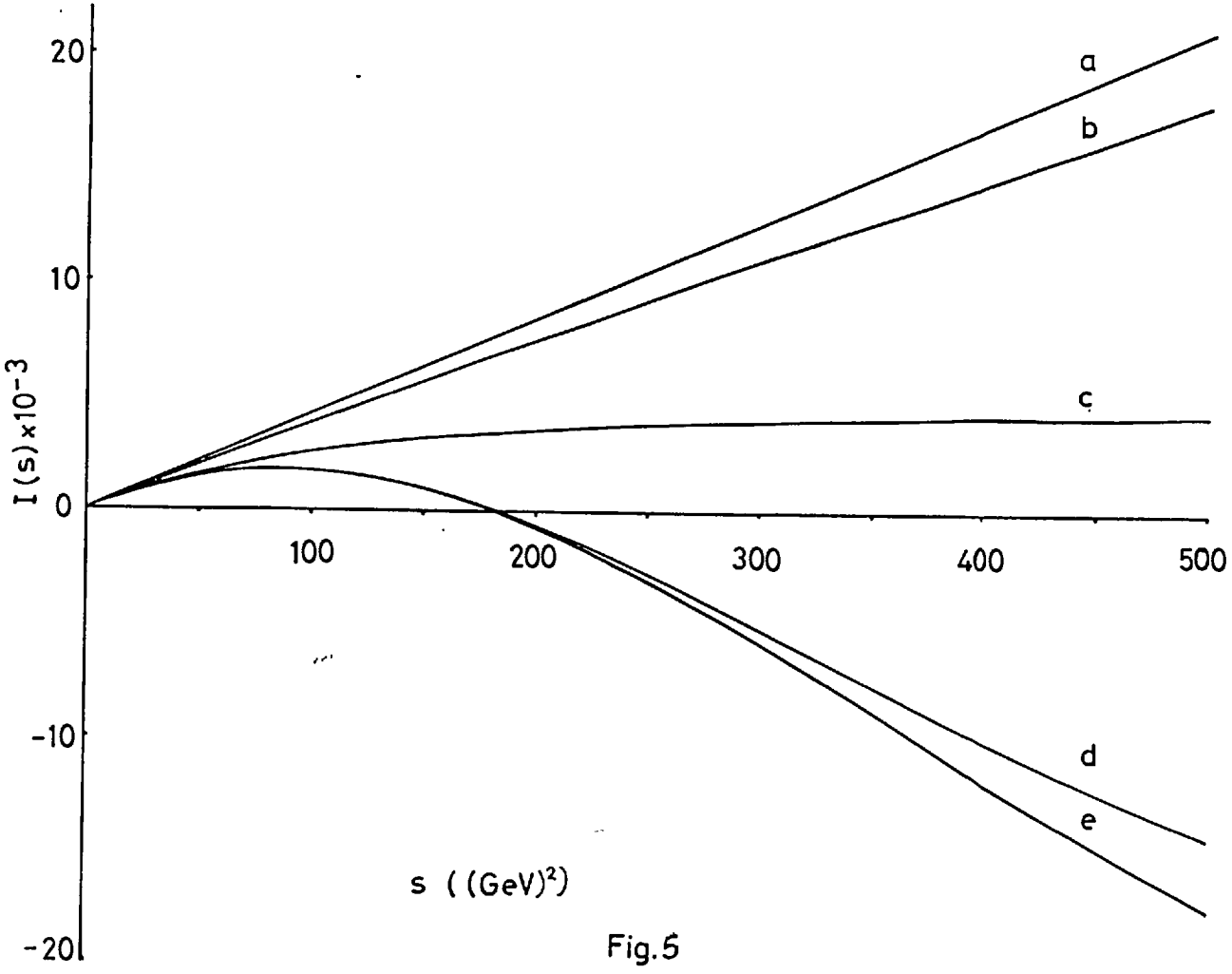

Fig.5

is crucial in determining the high energy tail. This appears not to be the case for the low energy part, but this is because the maximum u' value is less than $1 GeV^2$, our minimum value for the cut-off.

An even more dramatic demonstration of the necessity of cutting off the u'integration is given in Fig. 5. Here we show the results of solving for the kernel for a maximum energy of 500 GeV^2. In this calculation we have, for technical reasons left out the resonance contribution to $\sigma_{tot.}$. The integrations are done by splitting up the range of integration into a set of discrete points. The function is calculated at each point and weighted according to a certain prescription, then the sum of these weighted values is the integral. Thus if the function being integrated is a rapidly varying function (like the resonant cross-section) there must be a large number of points to give a reasonable degree of accuracy. As we increase the maximum energy, fewer and fewer points lie in the resonance region, and the integration over this region becomes very inaccurate. We therefore neglect this part of cross-section. To check whether this has a serious effect on the results we boosted the value of some of the lower points. While the numbers changed slightly, the character of the solutions remained the same.

Curve a is again the Pomeron contribution $\alpha k \sqrt{s}\, \sigma_{tot}^{I=0}$.

Curves b,c,d and e correspond to u'-cut-offs at 1, 10, 100 and ∞ GeV^2 respectively. Note that the last two become negative at high s.

On increasing the maximum energy even more, the solution e was found to oscillate in sign, with an amplitude that increases faster than the input function (Fig. 6). This is rather an unexpected feature, as unitarity demands that the irreducible kernel should be positive for all $s > 4m_\pi^2$. It is clear then that the off-mass-shell effects are very important and must occur in such a way that the kernel comes out

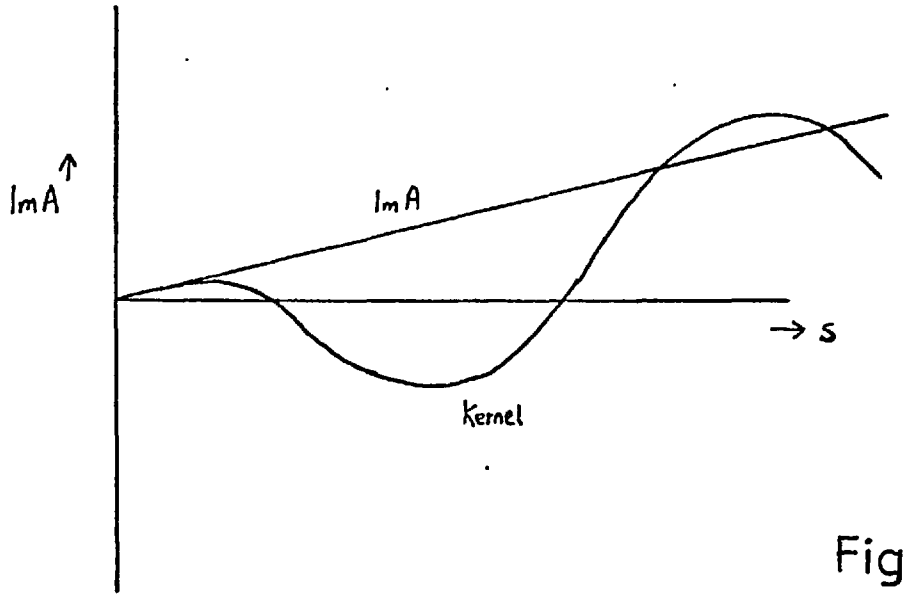

Fig. 6

positive. A cut-off at $1GeV^2$ kept the kernel positive, and of the same order as the input to $s \sim 10{,}000\ GeV^2$, with no indication of a turn-over. This is vastly different from CRS's guess.

Technically the calculation of the kernel involves subtracting two large numbers. To check that our curves do not result from instabilities in the computer program, the kernel we obtained was fed back into the integral equation and gave the original input to within a few per cent. We also checked to see whether the program would have found a kernel which tended to zero, by feeding in a single resonance, and resolving for the resonance. This was obtained with a few per cent accuracy.

Our conclusions are rather negative, in that, since we have no reliable, well-tested prescription for continuing amplitudes off-shell, it is difficult to guess what the input kernel corresponds to physically. If we still believe that the kernel should correspond to σ_{el}, the off-mass-shell effects must be such as to drastically increase the size and change the shape. In particular the low energy part of the kernel looks much more like σ_{tot} than σ_{el}.

REFERENCES:

1) R.P.Feynman: in "High Energy Collisions" (Gordon and Breach 1969) p. 237, and Phys. Rev. Letts. 23, 1415 (1969)

2) J.Benecke, T.T.Chou, C.N.Yang, and E.Yen; Phys. Rev. 188,2159 , (1969)

3) D.Amati, A.Stanghellini, and S.Fubini; Nuovo Cimento 26, 896, (1962)

4) See for example H.Satz: Rapporteur's talk at the Amsterdam Conference (Conference Proceedings edited by A.Tenner and M.Veltman, North Holland 1972.)

5) C.E.de Tar: Phys. Rev. D3, 128, (1971).

6) D.Silverman and Chung- I.Tan: Nuovo Cimento 2A, 489, (1971).

7) A.H.Mueller: Phys. Rev. D2, 2963, (1970).

8) H.P.Stapp: Phys. Rev. D3, 3177, (1971).

9) Chung-I.Tan: Phys. Rev D4, 2412, (1971).

10) J.C.Polkinghorne: Nuovo Cimento 7A, 555, (1972).

11) G.F.Chew: "The Analytic S-Matrix" (Benjamin 1966), and R.J.Eden, P.V.Landshoff, D.I.Olive, and J.C.Polkinghorne: "The Analytic S-Matrix" (Cambridge University Press 1966).

12) C.E.de Tar, C.E.Jones, F.E.Low, J.H.Weis, J.E.Young, and Chung-I Tan: Phys. Rev. Letts. 26, 675, (1971).

13) H.M.Chan, C.S.Hsue, C.Quigg, and J.M.Wang: Phys. Rev. Letts. 26, 672, (1971).

14) H.Harari: Phys. Rev. Letts. 20, 1395, (1968).

15) P.G.O.Freund: Phys. Rev. Letts. 20, 235, (1968).

16) R.C.Arnold: " Lectures on Inclusive Reactions " Argonne preprint ANL/HEP 7139 November 1971.

17) E.L.Berger: " Phenomenology of Inclusive Reactions " Argonne preprint ANL/HEP 7134 July 1971.

18) E.L.Berger: " Inclusive Reactions - A Second Glance " Argonne preprint ANL/HEP 7148 October 1971

19) Aachen - Berlin - Bonn - CERN - Cracow - Heidelberg - Warsaw collaboration: CERN report no. CERN/D.Ph II/PHYS/71 (June 1971)

20) M.S.Chen et al: Phys.Rev. Letts. 26, 1585 (1971).

21) L.G.Ratner, R.Ellis, G.Vannini, B.A.Babcock, A.D.Krisch, and J.B.Roberts: Phys. Rev. Letts. 27, 68, (1971).

22) G.Barbiellini et al : Physics Letts. 39B, 294, (1972).

23) G.W.Parry: Nucl. Phys. B37, 477 (1972).

24) V.V.Sudakov: Žum. Éksp. Teor. Fiz. 30 ,87, (1956).

25) I.G.Halliday and L.M.Saunders: Nuovo Cimento 60A, 115, (1969).

26) For a complete list of references see G.F.Chew and A.Pignotti: Phys. Rev. 176, 2112, (1968).

27) I.G.Halliday: Nucl. Phys. B33, 285, (1971).

28) I.G.Halliday and G.W.Parry: Nucl. Phys. B36, (1972).

29) M.Le Bellac: Physics Letts. 37B, 413, (1971).

30) J.Finkelstein and K.Kajantie: Nuovo Cimento 56, 659, (1968).

31) D.Z.Freedman, C.E.Jones, F.E.Low and J.E.Young: Phys. Rev. Letts. 26, 1197, (1971).

32) See for example Ref. 26.

33) See for example Ref. 12.

34) H.D.I.Abarbanel: Phys. Rev. D3, 2227, (1971).

35) Chian-Li Jen, Hyungsik Kang, Pu Shen and Chung-I. Tan: Phys. Rev. Letts. 27, 458, (1971).

36) For references on the eikonal model see for example M.M.Islam - lectures delivered at the Boulder summer school 1971.

37) V.N.Gribov: Soviet Physics - JETP 26, 414, (1969).

38) I.T.Drummond: Phys. Rev. 176, 2003, (1968).

39) D.K.Campbell: Phys. Rev. 188, 2471, (1969).

40) J.C.Botke: " Multi Reggeon Effects for Inclusive Reactions in the Pionzation Region " Cambridge University preprint DAMPT 71/44 December 1971.

41) J.H.Weis: Phys. Rev. D4, 1777, (1971).

42) D.M.Tow: Phys. Rev. D2, 154, (1970).

43) See for example P.Rotelli: Imperial College preprint ICTP/70/31 July 1971 for a discussion and some references.

44) G.F.Chew and A.Pignotti: Phys. Rev. 180, 2112, (1968).

45) C.P.Wang: Phys. Rev. 180, 1463, (1969).

46) B.R.Webber: " Multiplicities and Correlations in Hadron Production Processes ", Cambridge University, Cavendish Laboratory preprint March 1972.

47) W.D.Shepherd, J.T.Powers, N.N.Biswas, N.M.Cason, V.P.Kenney and D.W.Thomas: Phys. Rev. Letts. 28, 703, (1972).

48) A.H.Mueller: Phys. Rev. D4, 150, (1970).

49) L.S.Brown: Phys. Rev. D5, 748, (1972).

50) F.Predazzi and G.Veneziano: CERN preprint TH 1378 (1971).

51) A.Bassetto, M.Toller, and L.Sertorio: Nucl. Phys. B34, 1 (1971).

52) L.Bertocchi, S.Fubini, and M.Tonin: Nuovo Cimento 25, 626, (1962).

53) G.F.Chew, T.Rogers and D.R.Snider: Phys. Rev. D2, 765, (1970).

54) J.D.Jackson, J.T.Donahue, K.Gottfried, B.Svensson and R.Keyser: Phys, Rev. 139B, 428, (1965).

55) E.Ferrari and F.Selleri: Nuovo Cimento Suppl. 24, 453, (1962).

56) M.L.Goldberger: Varrena summer school lecture notes July 1971.

57) J.W.Dash: i) " Analytic Strong Coupling solutions of the ABFST Equation ", Nuovo Cimento (to be published).

and ii) Nuovo Cimento 8A, 787, (1972).

58) See for example L.Caneschi and R.Schwimmer: Phys. Rev. D3, 1588, (1971).

59) L.W.Jones et al : Phys. Rev. Letts. 25, 1679, (1970).

60) A.Bialas, K.Fialkowski and K.Zalewski: Jagellonian University preprint TPJU - 5 72 March 1972 , where other references may be found.

61) E.L.Berger, B.Y.Oh and G.A.Smith: Argonne preprint ANL/HEP7209 March 1972.

62) J.W.Dash: private communication.

63) G.F.Chew and D.R.Snider: Phys. Rev. D1, 3453, (1970).

64) G.F.Chew and D.R.Snider: Phys. Rev.D3, 420, (1971).

65) J.W.Dash, J.R.Fulco and A.Pignotti: Phys. Rev. D1, 3164, (1970).

66) G.F.Chew and W.R.Frazer: Phys. Rev. 181, 1914, (1969).

67) This seems to be the case - see for example ref. 63.

68) W.R.Frazer and C.H.Mehta: Phys. Rev. D1, 696, (1970).

69) D.R.Snider and D.M.Tow : Phys. Rev. D3, 996, (1971).

70) A.Jurewicz et al: Nucl. Phys. B29, 269, (1971).

71) H.W.Wyld: " Multiperipheral bootstrap model with SU(3) multiplets " CERN preprint TH - 1361-CERN July 1971.

72) D.R.Avalos and B.R.Webber: Phys. Rev. D4, 3313, (1971).

73) I.G.Halliday, S.Islam and G.W.Parry: " The ABFST equation and High Energy Scattering " , J.Phys. A (to be published).

74) J.D.Jackson: Nuovo Cimento 34, 1644, (1964).

75) H.D.I.Abarbanel, G.F.Chew, M.L.Goldberger, and L.M.Saunders: Phys. Rev. Letts. 25, 1735, (1970).

APPENDIX

THE NUMERICAL SOLUTION OF A VOLTERRA EQUATION

Our equation is

$$f(s) = g(s) \mp \int_{s_0}^{s} ds' \, K(s,s') f(s') \qquad \text{A.1}$$

The equation has a uniformly, absolutely convergent Neumann series solution for all finite s

$$f(s) - g(s) \mp \int_{s_0}^{s} ds' \, K(s,s') g(s') + \int_{s_0}^{s} ds'' K(s,s'') \int_{s_0}^{s''} K(s'',s') \, g(s') ds' \mp \cdots \qquad \text{A.2}$$

Clearly, if we write $g(s) = \hat{g}(s)$ where $\hat{g}(s) = 0$ for $s > M^2$ but $g(s) = \hat{g}(s)$ for $s < M^2$ then solve

$$\hat{f} = \hat{g} \mp \int K \hat{f} \qquad \text{A.3}$$

we find $\hat{f} = f$ for $s < M^2$ A.4

Thus we pick an upper bound for all energies s. The integral is approximated by a finite sum

$$\int ds' \, K(s,s') ds' = \sum_{j<i} K_{ij} \, WT(j) f_j \qquad \text{A.5}$$

where $s_{i+1} > s_i$ and $f_j = f(s_j)$.

$WT(j)$ is the weight attached to the j'th point in quadrature.

$$K_{ij} = K(s_i, s_j') \qquad \text{A.6}$$

Let

$$\hat{K}_{ij} = K_{ij} \, WT(j) \qquad \text{A.7}$$

then $f_i = g_i \mp \hat{K}_{ij} f_j$

or $[\delta_{ij} \pm \hat{K}_{ij}] f_j = g_i$ A.8

Now $\hat{K}_{ij} = 0$ if $j > i$ since the equation is Volterra.

The matrix $\hat{K}_{ij}$ is therefore lower triangular (Fig. 1).

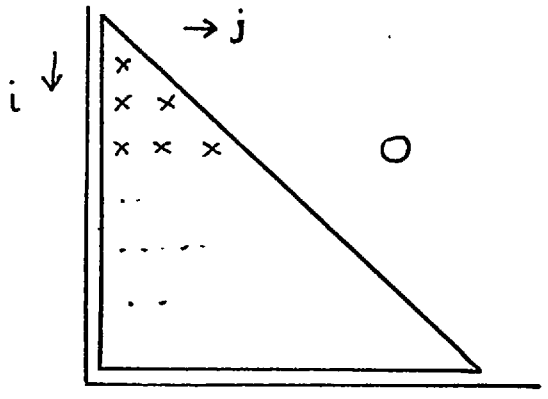

Fig. 1

Calling $\delta_{ij} \pm \hat{K}_{ij} = D_{ij}$ we have

$$f_1 = g_1 / D_{11} \ ,$$

$$D_{21} f_1 + D_{22} f_2 = g_2 \quad \Rightarrow \quad f_2 = \frac{g_2 - D_{21} f_1}{D_{22}} \ ,$$

$$f_i = \frac{g_i - D_{i1} f_1 - D_{i2} f_2 - \cdots}{D_{ii}} \qquad \text{A.9}$$